Chapter1

Introduction

1-1: Magnetic materials and semiconductors

With the continuous progress in modern technology, magnetic materials have become more attractive and important in various industrial applications, such as numerous electronic devices, magnetic recording equipments, magnetic sensors, and magnetoresistance read heads, and so on. Recent researches have been directed particularly to spin electronics, colossal magnetoresistances, tunneling current diodes, and etc. More recently, multiferroics have attracted extensive interest due to the significant magnetoelectric effect exhibited in these materials. In that, the electrical polarization and magnetization can be controlled by applying magnetic and electric fields, respectively, which might result in remarkable application potential in the field of data storage, such as non-transient memory and non-volatile memory (NVM).

In most of the above mentioned applications, the basic operation mechanism is implemented by regulating the electric currents in the channel with the applied electric field. This causes large power consumption and limited rate of operation.

Consequently, in order to achieve faster operation and multifunction need, design and fabrication of nano-size devices are imperative. However, in the nanometer scale, the exchange interactions between electron-electron, and electron-phonon, are predominant and full consideration is necessary. Especially, if the device operation can be based on the mechanism of using electron spins, the operation speed can be enhanced with much lower power consumption. The combination of the two conventional domains, magnetic materials and electronics, thus has become a popular issue both in academic and in industrial research and was termed as spintronics **[1, 2].**

However, in order to implement the ideas of various spintronic devices, semiconductors with room temperature ferromagnetism appears to the important ingredient. If we find such materials, it would create more opportunities toward the realization of the proposed novel spintronic devices. On the other hand, exotic mechanisms leading to room temperature ferromagnetism are also under extensive researches worldwide. For instance, recently several teams have found that there are magnetic phenomena in the absence of magnetic elements doping.

This seems to indicate that the involvement of magnetic atoms is not the only possible way of obtaining magnetism in a material. Therefore, the basic definition of DMS may need to be revised.

1-2 Diluted Magnetic Semiconductors (DMSs)

1-2.1 What's DMS?

Literally speaking,

"Diluted" means small doping concentration (a few %);

"Magnetic" means the display of ferromagnetism;

"Semiconductor" means that the matrix used is primarily a semiconductor.

Generally speaking, a diluted magnetic semiconductor (DMS) is a semiconductor doped with relatively small amount of magnetic atoms. The most studied systems are II-VI and III-V semiconductors, as well as wide-band gap oxides (ZnO, TiO_2) doped with magnetic elements such as Mn, Cr, Fe and so on. In these systems, the partially-filled orbital electrons are playing the most prominent role in magnetism while presewing most of the semiconducting properties of the host matrix material. That is to say, the semiconductor in which a fraction of the host cations can be substitutionally replaced by magnetic ions or

appropriate rare earth elements. As for how to make nonmagnetic semiconductor magnetic? **[3]** The usefulness of semiconductor largely resides in the versatility of doping with various kinds of impurities to change their properties. For instance, this approach can be followed by introducing magnetic elements into nonmagnetic semiconductors to make them magnetic. Fig.1.1 schematically displays the pictorial presentation of magnetic semiconductor **(Fig. 1.1(A))**, diluted magnetic semiconductor **(Fig. 1.1(B))**, and nonmagnetic semiconductor **(Fig. 1.1(C)) [4]**.

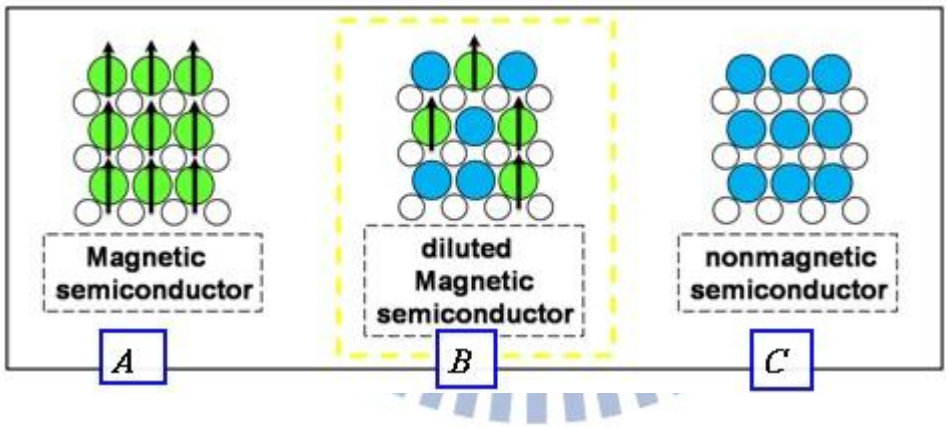

Fig. 1.1 Schematic illustration of (**A**) magnetic semiconductor (B) diluted magnetic semiconductor; and (**C**) nonmagnetic semiconductor.

1-2.2 Types of DMSs

Generally speaking, there are three types of DMS materials. Namely, magnetic ion-doped II-VI and III-V semiconductors, as well as TM-doped oxides. Among them, ZnO and TiO_2 are receiving extensive attention as the potential host materials for obtaining room-temperature ferromagnetism (RTFM).

In early years, study of DMSs and their heterostructures have centered mostly on **II-VI semiconductors**, such as CdTe and ZnSe, in which the valence of the cations matches that of the common magnetic ions such as Mn. Although this phenomenon makes these DMSs relatively easy to prepare in bulk form as well as in thin epitaxial layers, II-VI based DMSs have been difficult to dope into *p-type* or *n*-type, which made the materials less attractive for applications. Moreover, the magnetic interaction in II-VI DMSs is dominated by the antiferromagnetic exchange coupling among the Mn spins. As a result, the materials mostly exhibit paramagnetism, antiferromagnetism, or spin-glass behavior. Until very recent the II-VI DMS only became ferromagnetic at low temperature (2 K) **[5].**

The **III-V semiconductors** such as GaAs are already in use in a wide variety of electronic equipments in the form of electronic and optoelectronic devices, including cellular phones, microwave transistors, compact disks, semiconductor lasers, and so on. Therefore, the introduction of magnetic III-V semiconductors opens up the possibility of incorporate magnetism with a wide variety of existing applications derived from conventional nonmagnetic III-V semiconductors.

The representative oxide semiconductors of current interest are ZnO, In_2O_3, TiO_2 and SnO_2. These materials are normally n-type semiconductors because of then specific electronic structures. Their cations have filled d and empty s orbitals, and the conduction band and valence band are mainly formed by the empty metal s orbital and filled oxygen 2p orbitals, respectively. Owing to the special electronic structure, oxide DMSs **[6]** derived from these oxides are utilizing their unique properties such as large bandgaps, wide controllability of carrier concentration, and great flexibility in impurity ion doping.

Brief comparisons among the three types of DMSs are summarized in the following **(Fig. 1.2(a)).**

Fig. 1.2(a) Comparisons of II-VI DMSs, III-V DMSs, and oxides.

	II-VI (Mn-ZnTe)	III-V (Mn-GaAs)	Oxide(ZnO,TiO_2,GaN)
advantages	1 The same valence 2 High-density magnetic atoms	1 Easy to form n- or p-type 2 Ferromagnetic (FM)	1 Large bandgaps 2 Wide controllability 3 Great flexibility in impurity ion doping
disadvantages	1 Hard to form n- or p-type 2 Paramagnetic or Anti-FM 3 Tc is very low	1 Difficult to substitute cations 2 Second phase or cluster 3 Tc is higher, but still small	1 Insulators 2 Less conductivity

1-2.3 The development of DMSs

In 1960s, magnetic semiconductors, such as Eu- and Mn- chalcogenides and Cr spinels possessing both ferromagnetism and semiconducting characteristics were extensively studied. However, the ferromagnetic Curie temperature (Tc), of these materials were very low (about 10K-100K) and were very difficult to grow. Therefore, the attention has been to DMSs.

In 1980s, most of researches in DMSs have been focused on the II-VI semiconductors. Take the (Cd or Mn)Te, (Zn or Mn)Te, (Zn or Co)S, (Hg or Fe)Se for instance, although high density of magnetic atoms can be doped into the II-VI semiconductors, n -type or p- type doping carrier concentration remains relatively low due to transition metal elements have similar valences with cations of II-VI semiconductors. That is to say these materials only exhibit ferromagnetism below 10K, which has severely limited the development of II-VI semiconductors.

Later on, scientists had diverted the attention to the III-V semiconductors, such as $Mn_xGa_{1-x}As$. In that, Mn contributes both magnetic moments and hole carriers. Both turn out to be equally significant for obtaining ferromagnetism.

In 1989, Munekata used MBE to add Mn into InAs **[7, 8]**, and led to great progress on the research of DMSs.

In fact, Dietl et al. **[9]** theoretically predicted that in Mn-doped semiconductors, it is possible to obtain higher Curie temperature than room temperature, and in some wide bandgap host semiconductors also, as **Fig .1.2(c).**

In 2000, Ditel developed a theory to calculate the Curie temperature of various p-type semiconductors doped with 5% of Mn, and pointed out that gallium nitride (GaN) and zinc oxide (ZnO) have the change of achieving RTFM (**Fig. 1.2(b))**.

Indeed, over the past few years RTFM has been observed in p-type ZnO-based **[10]** as well as in Co: TiO_2 films **[11]**. Such observations have stimulated intensive experimental studies worldwide to look into the fundamental mechanism leads to RTFM in oxide DMSs.

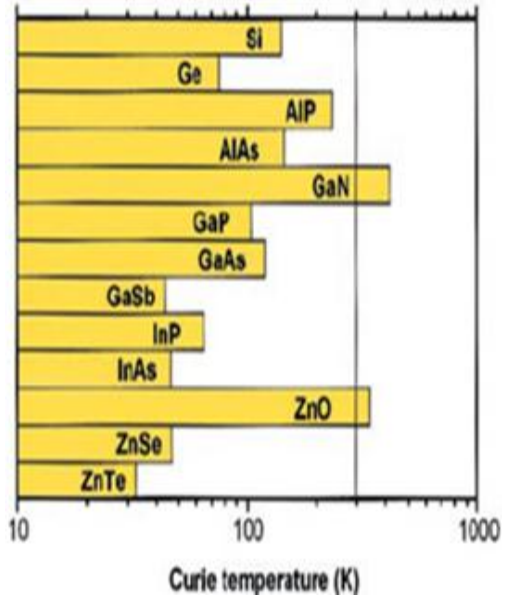

Computed values of the Curie temperature Tc for various p-type semiconductors containing 5% of Mn and 3.5×10^{20} holes per cm^3 [9].

Fig. 1.2 (b) Curie Temperature for various p-type semiconductors.

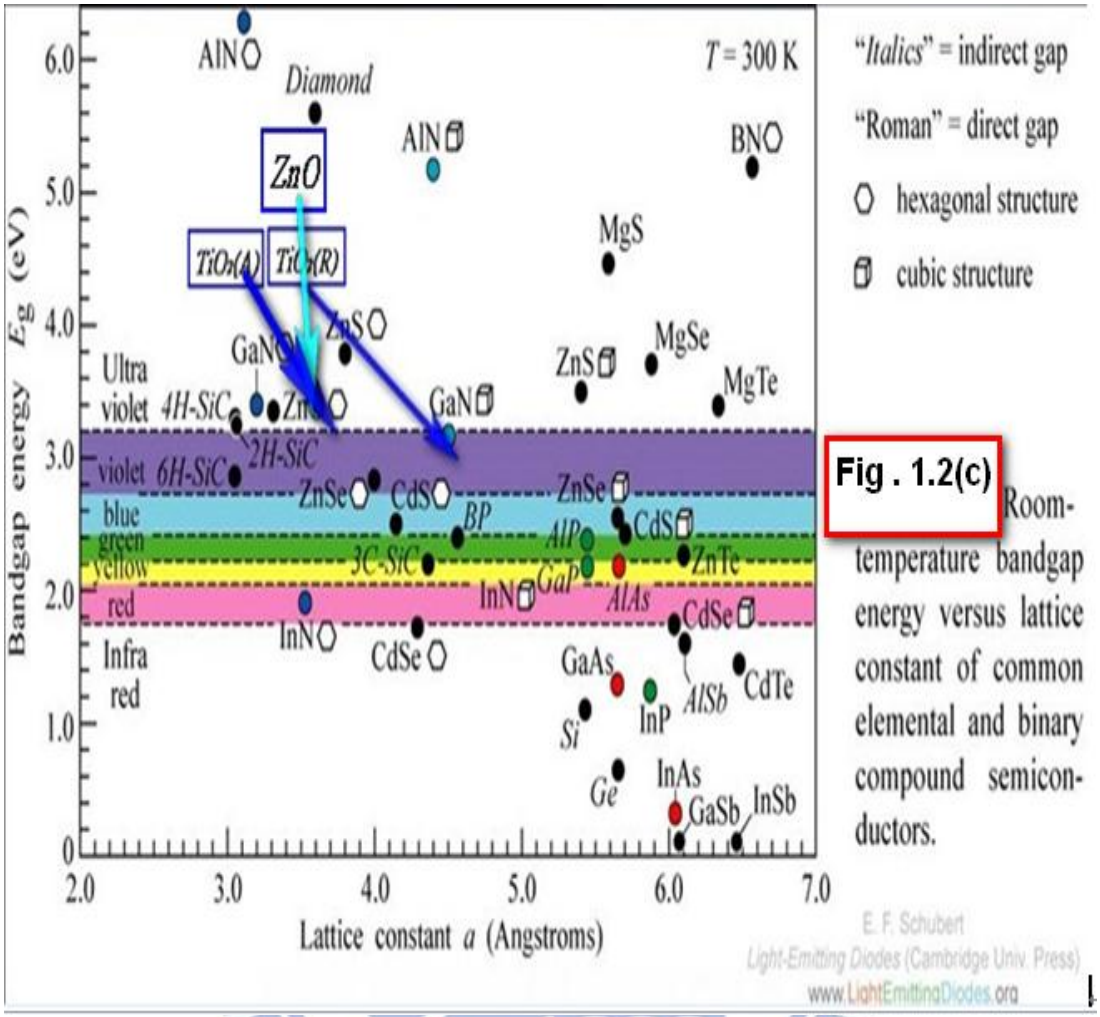

Fig . 1.2(c) Room-temperature bandgap energy versus lattice constant of common elemental and binary compound semiconductors.

Fig. 1.2(c) Bandgap versus lattice constant at room temperature for common elemental and binary compound semiconductors.

Fig .1.3 displays an example showing the RTFM in (Ga, Mn)N films deposited by MOCVD **(Fig. 1.3).**

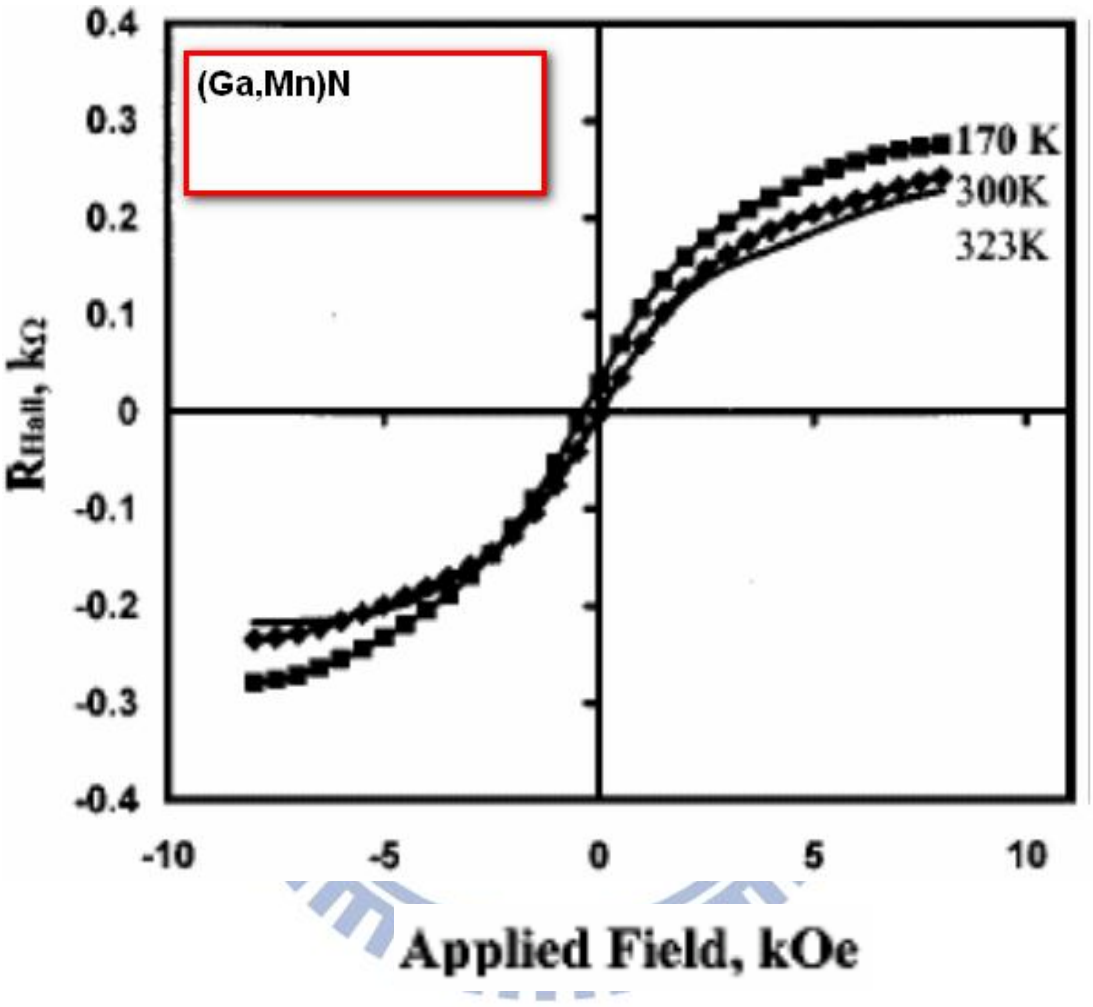

Fig. 1.3

Hall resistivity as a function of applied magnetic field measured at different temperatures for (Ga, Mn)N. **[12, 13].**

However, the results were somewhat controversial.

For instance, Sonoda et al. **[14]** prepared a 9% doping of (Ga, Mn)N film by MBE and reported a ferromagnetic Tc of ~940K **(Fig. 1.4(a))**. While Hashimoto et al. **[15]** used the similar techique to fabricate a 12% and 1.4% Mn-doped (Ga, Mn)N films only to observe a Tc of ~ 50K **(Fig. 1.4(b))**.

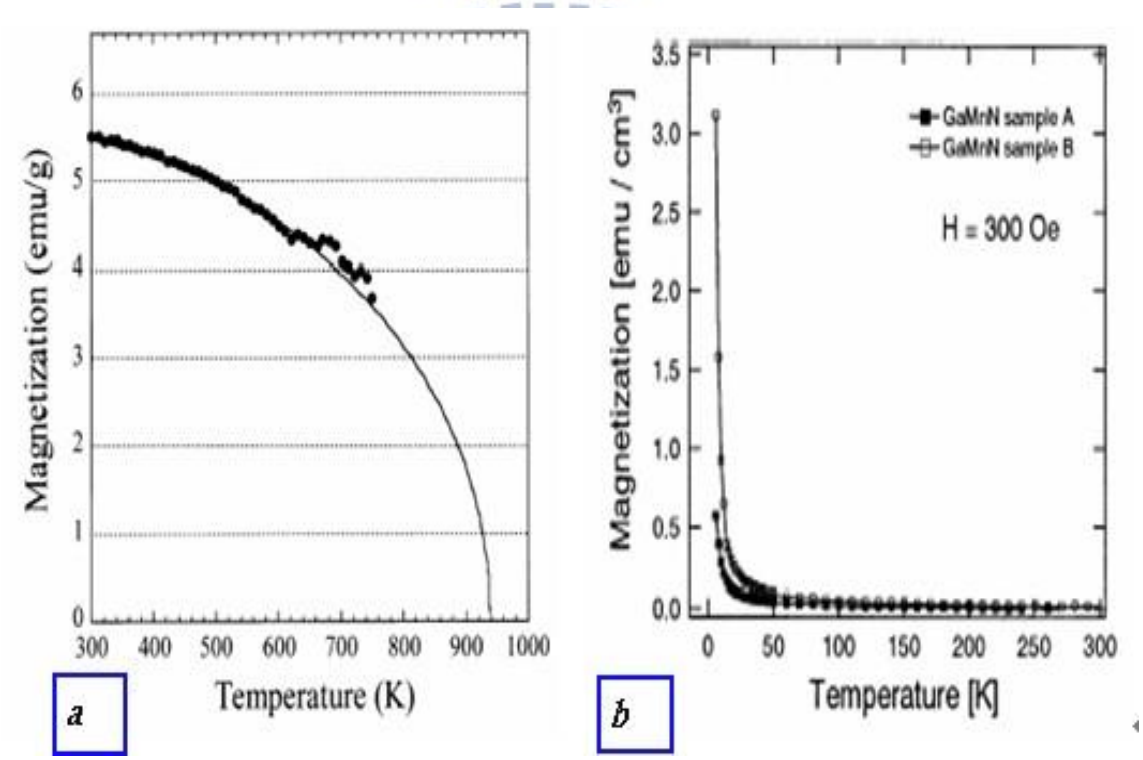

Fig. 1.4

The magnetization of (Ga, Mn)N with different doping concentrations

(a) The M-T curve of Mn-doped ratio of 9% by Sonoda **[14].**
(b) The M-T curves of Mn-doped ratio of A (12%) and B (1.4%) by Hashimo **[15].**

The reason for these apparent discrepancies is not well understood. However, the clustering of the doped magnetic Mn ions has been believed to play some role in this effect.

On the other hand, Ueda et al. **[16]** have extensively studied ZnO by doping it with Co, Mn, Cr, Ni and other elements. The Curie temperature up to 280K has been obtained for the Co-obtained ZnO **(Fig. 1.5).**

Whereas, sharma et al. **[17]** reported a Tc~=500 ^{o}C for ZnMnO fabricated by high-temperature sintering **(Fig. 1.6)**.

Although great progresses had been made in the development of DMSs, the results as mentioned above were not consistent,

And far from obtaining the optimized manufacturing conditions for practical DMSs **[18-23]**.

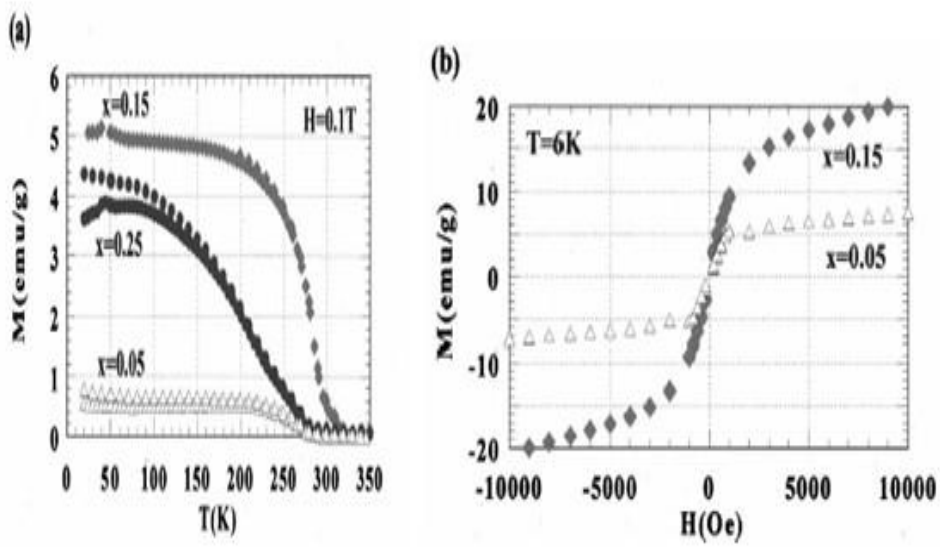

Fig. 1.5 $Zn_{1-x}Co_xO$ of (a) M-T Curves (b) M-H Curves **[16]**

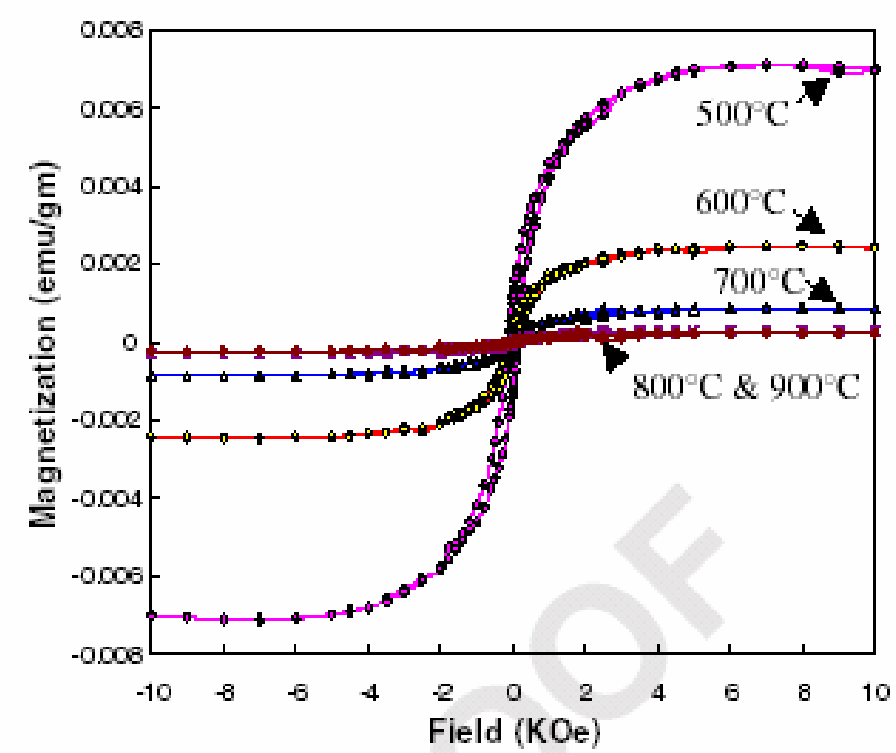

Fig. 1.6 M-H curves of sintered ZnMnO **[17].**

1-2.4 Why DMSs are so important?

As mentioned above, DMSs combine the electronic properties of semiconductor and magnetic properties of the doped magnetic atoms. The integration of electronics and magnetism might explore spin-correlated devices, and broaden the applications of these devices. Spintronics focused on how to effectively inject spins into semiconductor materials, to manipulate spin transport in the host semiconductor, and finally to detect these spins. If we can reach these goals, it will lead to enormous influences of the performance of spintronic devices.

So it is very important to understand the basic mechanisms for the spin injection, transport and detection.

1.3 Titanium dioxide

1.3-1 Photocatalyst

One of the mentioned oxide DMSs is titanium dioxide (TiO_2), which also has extensive applications in photocatalyst, due to its good oxidation ability, chemical stability and non-toxic **(Fig. 1.7)**. Since in 1972, it had become most popular material of nano photocatalysts, masks and other consumer goods.

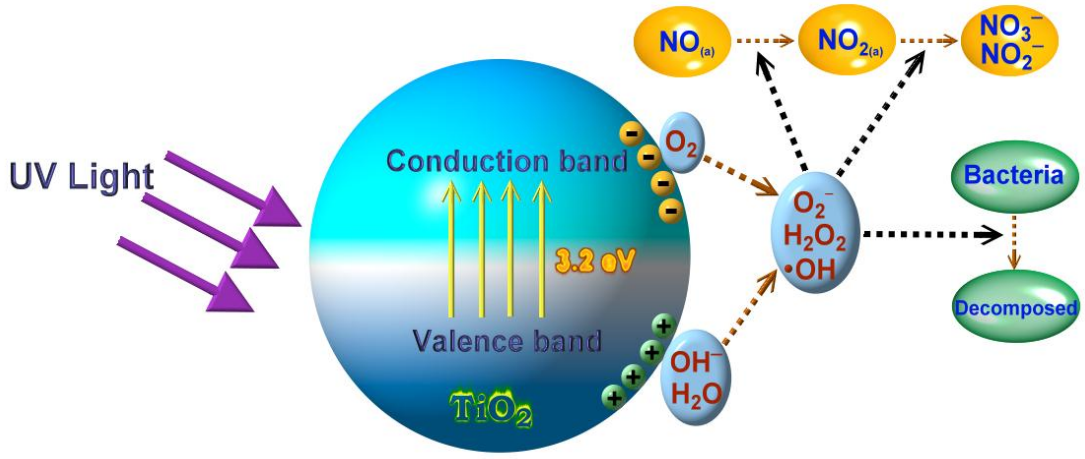

Fig. 1.7
Schematics showing the characteristics and applications of TiO_2.

1-3.2 Literature review of TiO_2

In 2001, Matsumoto et al. **[24]** used pulsed laser deposition (PLD) to mix Cobalt into anatase phase of TiO_2 and discovered that it can form a DMS with Tc was higher than 400K.

This result was published in *Science* and attracted a lot of attention from many researchers. Then, Chambers et al. **[25]** used oxygen-plasma-assisted molecular beam epitaxy (OPAMBE) system to make Co-doped anatase phase TiO_2 also found RTFM. More recently, two teams of Matsumoto **[26]** and Park **[27]** used reactive sputtering and PLD also found RTFM in Co-doped TiO_2 of rutile phase. In these experiments, we can get RTFM as long as the doping concentration reaches 1%. Consequently, the origin of RTFM observed in these oxide systems is still a matter of extensive debate **[28]**.

It has been pointed out that the magnetic contribution at room temperature is likely originated from Cobalt clusters existing in the Co-doped TiO_2,

as evidenced in the TEM micrograph shown in **Fig. 1.8 [29].**

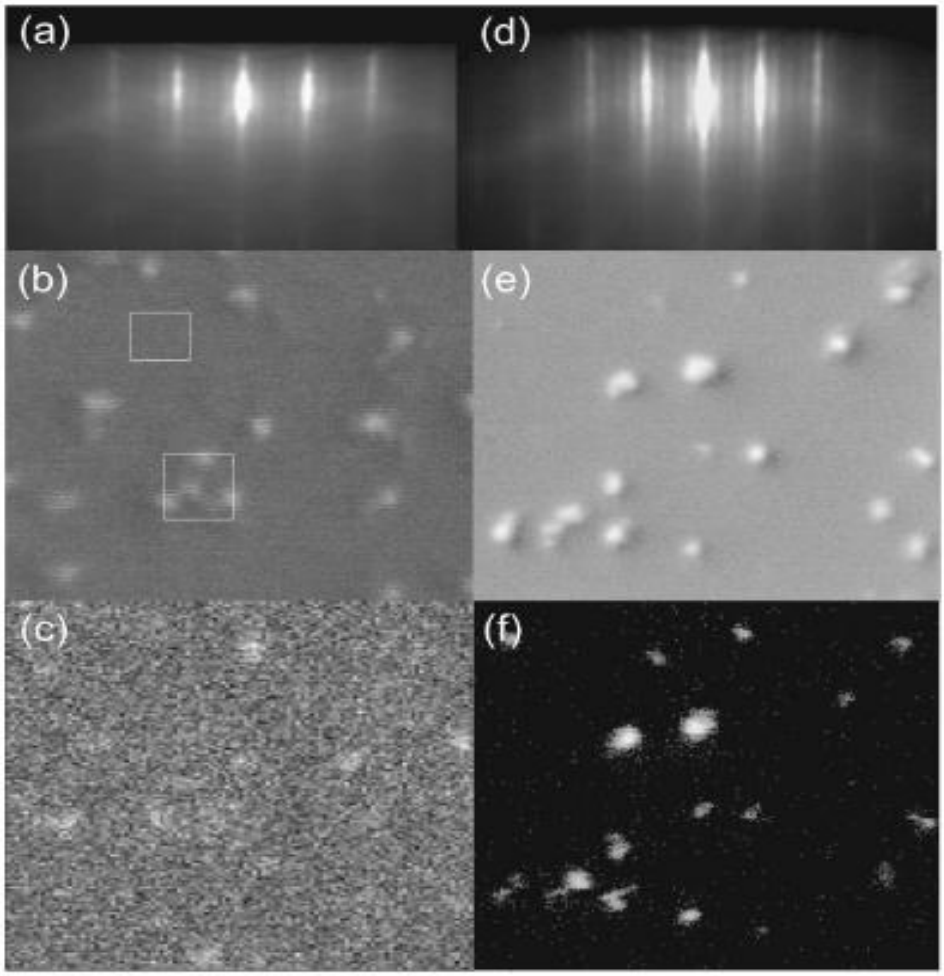

Fig. 1.8 Images of the OPAMBE growth of $Co_xTi_{(1-x)}O_2$ single crystal film from RHEED (a and d), SEM (b and e) and Auger intensity maps (c and f) **[29].**

On the other hand, Puoose et al. **[30]** performed zero field cooling (ZFC) and field cooling (FC) magnetization measurements to demonstrate that all samples, in fact, exhibited magnetic particle blocking phenomenon in the course of ZFC, as shown in **Fig. 1.9**.

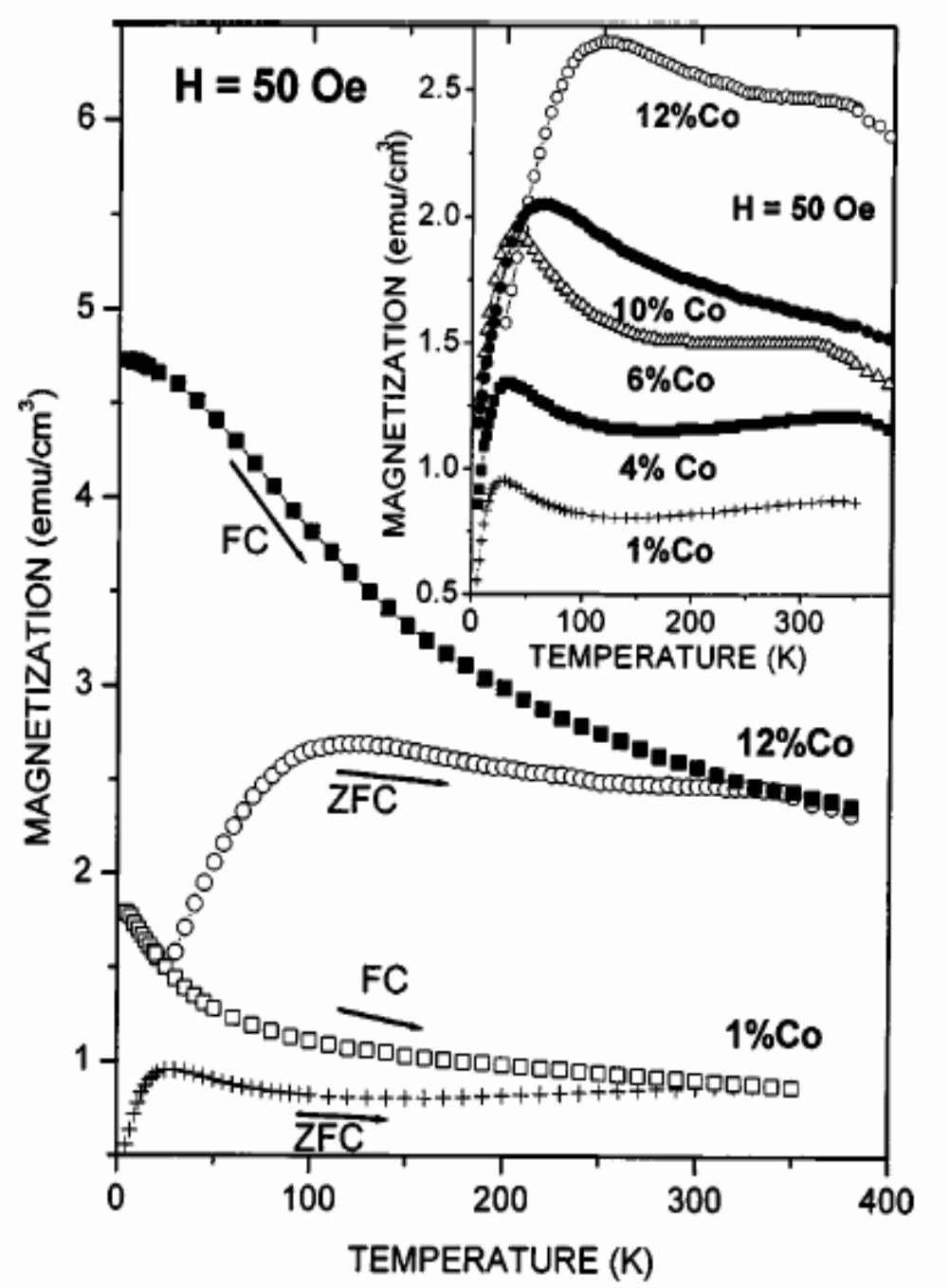

Fig. 1.9 The M-T (ZFC-FC) curves of $Co_xTi_{(1-x)}O_2$ thin films with $0.01 \leq x \leq 0.12$ **[30]**.

Moreover, the temperature-dependence of the resistance measured by Kennedy et al. **[31]** also displayed multiphase transition behavior, indicating the existence of Co-clusters.

However, Hong et al. **[32]** showed that the vanadium (V)-doped anatase phase of TiO_2 not only exhibited higher magnetic moment than the Co-doped anatase phase of TiO_2 but also showed no detectable nanoparticles or clusters, as displayed in **Fig. 1.10**.

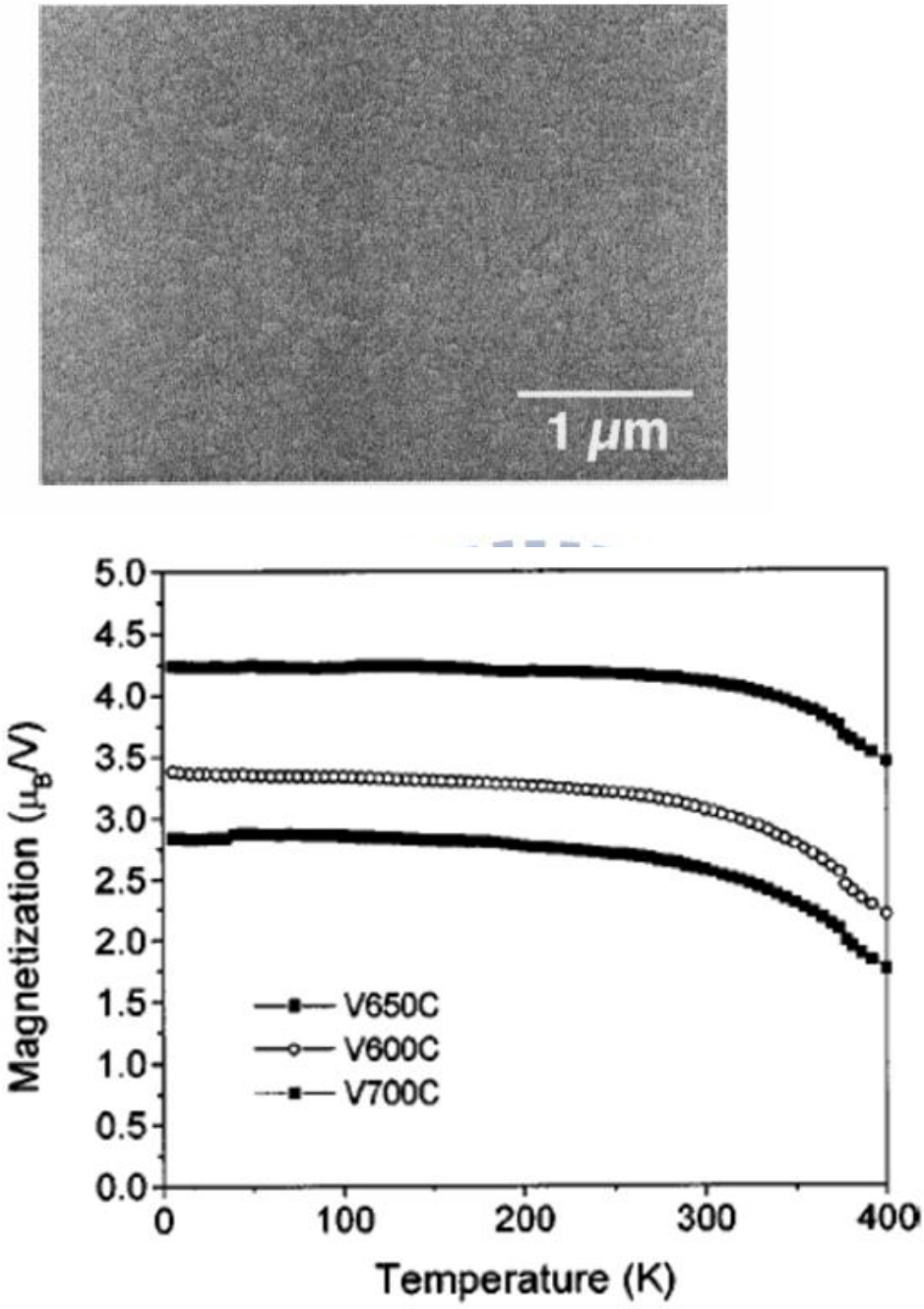

Fig. 1.10 **[32]**

(a) SEM image of $Ti_{0.95}V_{0.05}$ O_2 grown at 700℃

It has no detectable nanoparticles or clusters.

(b) M-T curves of $Ti_{0.95}V_{0.05}$ O_2 at different growth temperatures.

In recent years, more research results have been reported on obtaining RTFM in Co-doped anatase phase TiO_2 **[33, 34].**

In these cases, no Co clusters or other mixed phases were detected by X-ray diffraction, high resolution TEM, and X-ray absorption spectroscopy (XAS) analysis, which further confirmed that the source of magnetism mainly come from the substitution of Co **[33]** or Ni **[34]** at Ti sites in TiO_2. Therefore, it appeared that the development of the diluted magnetic semiconductors have successfully overcome the problems of sub-room-Curie Temperature (Tc) and controversies of phases originated from doped transition metals. The question remained to be asked is what's the origin of RTFM observed in these systems, is it was not from magnetic clusters? Among many theories that have been proposed, the bound magnetic polaron (BMP), direct exchange, double exchange, and super exchange models, we will briefly introduced in Chap. 2.

Following is a summary of development of TiO_2

2001 Matsumoto	Co-doped Anatase-TiO_2 $T_c > 400K$
Park & Matsumoto	Co-doped Rutile-TiO_2
2004 N.H. Hong	V-doped A-TiO_2 and Ni-doped TiO_2
2005 K.A. Griffin	Co-doped A-TiO_2
2006 N.H. Hong	un-doped TiO_2 **[35]**
2010 G. Drera et all	Nitrogen-doped TiO_2

1-3.3 The crystal structure of titanium dioxide

In nature, the titanium dioxide has three kinds of crystal structures, the first is anatase, the second is rutile, and the last is brookite. Generally speaking, brookite is not stable and seldom to exist in nature, therefore, the research trend of TiO_2 usually focus on anatase and rutile.

Following **(Fig. 1.11)** shows structures of anatase and rutile.

Among the three structures, anatase and rutile are most common and also often used in photocatalytic reactions. Besides, rutile is more stable than anatase because the crystal structure is inside a dense accumulation of atoms. Comparatively, while the anatase phase meets high temperature, it will gradually transfer into rutile phase, that is to say rutile phase is easier to obtain, as for why we prefer to research anatase phase?

According to some researchs **[36]**, the photocatalytic activities, gas sensing characteristics and mobilities of charge carriers in anatase TiO_2 are better than that in rutile phase. Nevertheless, it has been pointed out that the mixed phase TiO_2 (anatase + rutile) has higher photocatalytic activity than the single anatase or rutile phase. Therefore, there are some researches trying to explore the potential of the mixed phase.

Crystal structure	Band gap (eV)	Absorption edge (nm)	Density (kg/m^3)	stability
Anatase	3.2	388	3830	metastable
Rutile	3.0	410	4240	stable
Brookite	3.4	359	4170	metastable

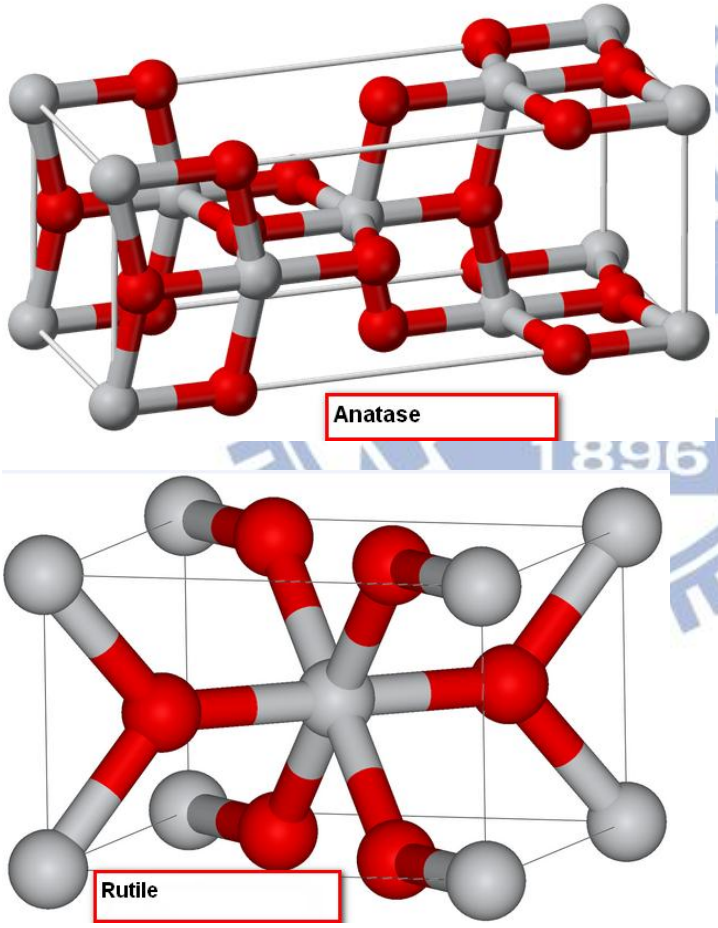

Fig. 1.11 Structures of anatase and rutile phase TiO_2.

Rutile is tetragonal (a = 4.59 Å and c = 2.96 Å) with a bandgap of 3 eV while the anatase phase also crystallizes in a tetragonal structure (a = 3.78 Å and c = 9.52 Å) with a bandgap of 3.2eV **[37]**.

1-3.4 TiO_2-based materials

Single phase TiO_2 thin films of either rutile or anatase structure can be prepared on $SrTiO_3$ (100) substrates by *in situ* PLD **[38]**. Epitaxial anatase thin films can also be fabricated on lattice-matched (0.2%) $LaAlO_3$ (100) substrates in the layer-by-layer fashion by laser MBE. In addition, X-ray diffraction (XRD) and transmission electron microscopy (TEM) show the films grown on $LaAlO_3$ (100) is able to exhibit high crystallinity and atomically defined interfaces with an optical bandgap of 3.3eV at room temperature **[39]**. As a result, the metastable anatase form of TiO_2 which is difficult to stabilize in bulk, but it can be grown in the form of thin films by choosing an appropriate lattice-matched substrate. Epitaxial rutile films can also be obtained when using $SrTiO_3$ (111) substrates **[40]**.

Anatase TiO_2 is a wide bandgap semiconductor with excellent optical transmission in the visible and near-infrared regions, a high refractive index, high dielectric constant (ε_r = 105 at 4.2 K) **[41]**, low tangential loss (tan $\delta = 10^{-7}$ at 4.2 K) **[42]** and useful properties of photocatalyst **[43, 44]**. Therefore, we prefer anatase TiO_2 as our material of research.

1-3.5 2p-light element doped DMSs

Generally speaking, the choice for the doping elements in DMS is normally about transition metal for the purpose of pursuing excellent ferromagnetism, but since several groups have found room temperature ferromagnetism in N doped ZnO and C doped ZnO films **[45-48]**, more and more people want to use 2p-light element to replace the transition metal because of the 2p-light element is more convenient to obtain. However, because the mechanism of ferromagnetism induced by 2p-light element doping is still unclear, the theories of traditional DMS can't be applied to 2p light element doped DMSs. Nevertheless, it is believed that the valence electrons in p orbit are possible to get the same or even more strong long-range exchange coupling interaction. Therefore, DMSs doped with 2p light elements can be weak ferromagnets in a highly ordered and low doping concentration **[49]**. Pan et al. believed that substitution of oxygen by nitrogen and carbon atoms induces oxygen vacancies and holes in oxygen 2p states which couple with carbon and nitrogen 2p states. The interaction between oxygen and 2p-light element (carbon or nitrogen), also known as the p-p interaction, is believed to give rise to similar effects of the p-d hybridization in TM-doped DMSs.

Indeed the density functional theory (DFT), calculation has indicated that ferromagnetism may be induced when substituting oxygen with carbon in the anatase TiO_2 **[50]**. In that, it was indicated that each carbon has spin-spin polarized 2p states in the band gap generating a magnetic moment of $2.0\mu_B$. Similarly, Rumaiz et al. **[51]** showed that nitrogen-doped titanium dioxide also led to RTFM and concluded that nitrogen-doping not only gives rise to polarized spin but also induces high concentration of oxygen vacancies, which plays important role in medicating the coupling between polarized spins. Coey et al. **[52]** also proposed a model for the ferromagnetism of doped oxide nanoparticales and related materials. Basically, the defective oxides are presumed to be the Stoner ferromagnets; the spontaneous Stoner ferromagnetism can arise in percolating defect-rich regions where charge transfer happens. Therefore, the 2p-light elements can be better alternatives for transition metals to produce ferromagnets in oxide semiconducting materials. In these 2p-light elements, especially the carbon is more popular than other elements, that is why more and more people dedicate to the researches of carbon-doped oxide DMSs.

1-4 Motivation

Nevertheless, most the studies about carbon-doped TiO_2 were mainly concentrated on area of photocatalyst, and thus were mostly in powder form. The motivation of this study is to delineate the properties and mechanisms of the ferromagnetism in C-doped TiO_2 films. In particular, we will focus on the anatase instead of rutile phase, to see how the carbon doping affects its electronic structure and hence integrate the magnetism and photocatalysis effects.

.

Chapter 2

Background

2-1 Brief introduction to magnetism

There are two sources of magnetic moment in the atomic structure, one is the orbital motion of electron around the nucleus; the other is the electron spin itself. On the other hand, although nuclear spin also contributes to magnetic moment, it is relative value is so small that we usually ignore it in the discussion of macroscopic magnetism.

The basic unit of the magnetic moment is defined as Bohr magneton (μ_B), which was calculated by Bohr's atomic modal. That is to say, the orbital motion of electrons around the nucleus will generate the smallest magnetic dipole moment:

$$\mu_B = -\frac{e}{2m}\hbar = 0.927\times10^{-20}\, erg/Oe \qquad (2.1)$$

Where m is mass of electron, $\hbar$ is planck constant.

$$\hbar \equiv \frac{h}{2\pi} = 1.054\ 571\ 68(18)\times10^{-34}\ \mathrm{J\cdot s},$$

With the hypothesis of angular momentum quantization proposed by Bohr, the orbital magnetic dipole moment can be written as

$$\vec{\mu}_l = -\frac{g_l \mu_B}{\hbar}\vec{L} \qquad (2.2)$$

Generally we call g-factors g_l "orbital g factor", and $g_l = 1$. The magnetic dipole moment produced by spin of electron also has a similar form with the magnetic dipole moment produced by orbital motion. We call it the spin magnetic dipole moment of the electron.

$$\vec{\mu}_s = -\frac{g_s \mu_B}{\hbar}\vec{S} \qquad (2.3)$$

The g_s is called "spin g factor". $g_s = 2$ was determined through Phipps and Taylor who used Stern-Gerlach experimental methods to observe the Zeeman effect of hydrogen atoms. Modern experiments use more actuarial spectrum to conduct measurements, confirming that the result of g_s indeed was 2.00232 as predicted.

Then, if we consider both orbital angular momentum (L) and the spin angular momentum (S) at the same time, according to the spin –orbital coupling effect, we can obtain the total angular momentum.

$$\vec{\mu}_J = -\frac{g\ \mu_B}{\hbar}\vec{J} \qquad (2.4)$$

The g is called "gyromagnetic factor". As for the questions: What's the source of magnetism? Which magnetic moment is the real source? We can judge by measuring g factor through gyromagnetic effects and ferromagnetic resonance.

The following is information on the “g” factor **(Fig. 2.1).**

We observe that the “g factor” values are near “two”, which proves that ferromagnetism is not only due to orbital motion, but also from the spin of electron.

Material	g’	g”
Fe	2.12~2.17	2.08
Co	2.22	2.18
Ni	2.2	2.09~2.19
Heusler alloy	2.01	2.00

Fig. 2.1 the g values of various magnetic materials.

g" is measured by the gyromagnetic experiments;

g ' is measured by the ferromagnetic resonance experiments.

2-2 Types of magnetism

Generally speaking, most magnetic materials can be classified into the following categories:

(1) Paramagnetism:

When there are no external magnetic fields, the internal magnetic moments of paramagnetic materials are in scattered state, meaning that the sum of all magnetic moments is zero; but when paramagnetic materials are applied with external magnetic fields, the intrinsic magnetic moments will tend to align with the external magnetic fields. **Fig. 2.2** shows the schematic illustration of paramagnetic materials, **Fig. 2.3** shows the relation of susceptibility and temperature of paramagnetic materials.

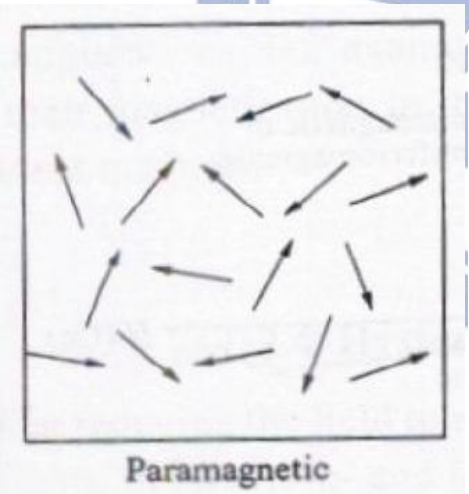

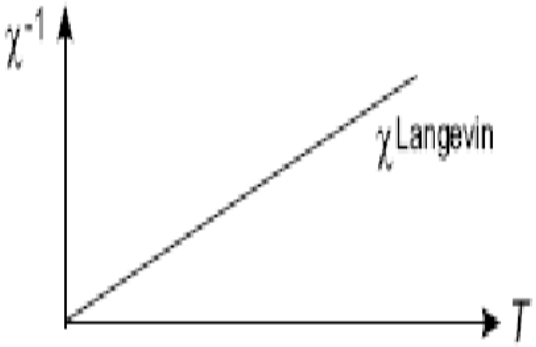

Fig. 2.2 The schematic illustration of paramagnetism.

Fig. 2.3 χ^{-1}-T curve of Langevin paramagnetism.

(2)Diamagnetism:

When materials with diamagnetism are applied by external magnetic fields, it will induce magnetic moments which are opposite to the direction of the applied magnetic fields. This characteristic is also called anti-magnetism.

Anti-magnetism represents the similar principle of Lenz's law, and has a strong relation with electron spin and rotation. **Fig. 2.4** shows the relation between susceptibility and temperature of paramagnetism and diamagnetism.

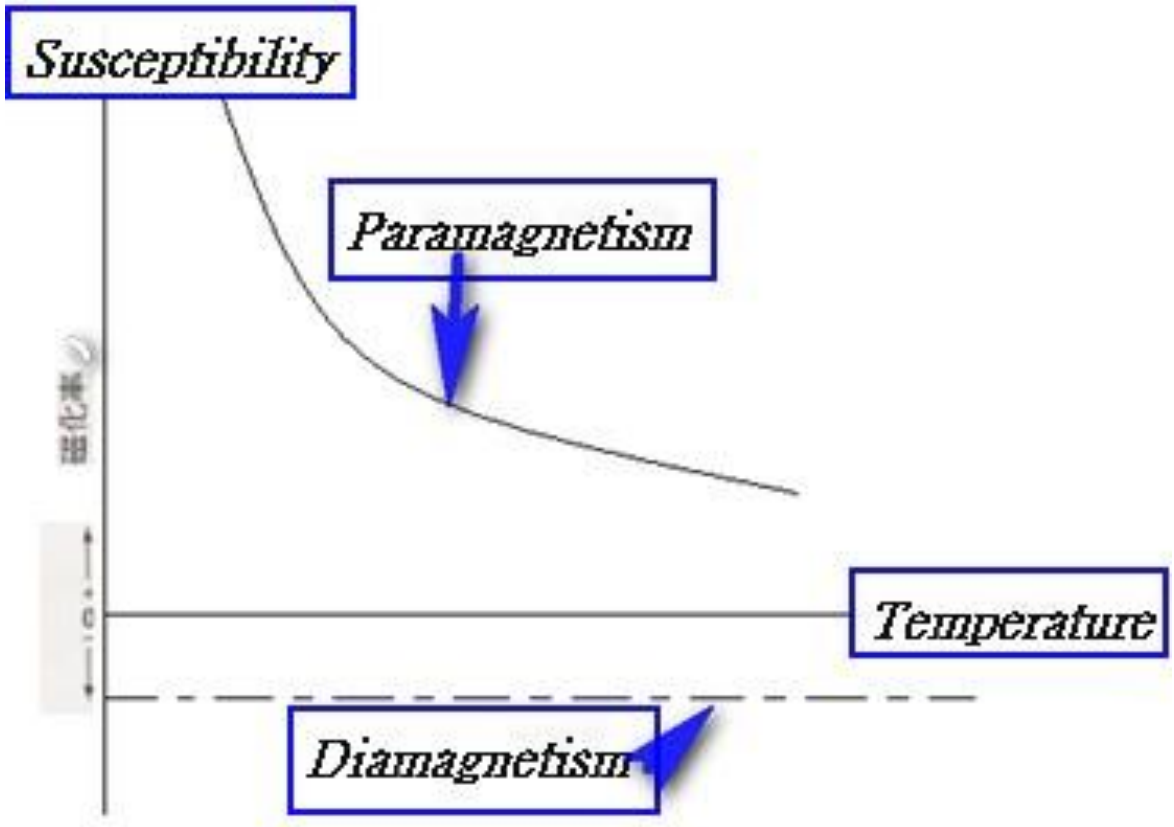

Fig. 2.4 Characteristics in magnetic susceptibilities of diamagnetism and paramagnetism.

(3)Ferromagnetism:

The magnetic moments of ferromagnetic materials arrange almost neatly in the same direction even without external magnetic fields. When we apply an external magnetic field, the ferromagnetism will appear, and the materials can be magnetized to saturation as long as a very weak magnetic field is applied. Besides, if it subjects to a magnetic field which is opposite to the previous direction, as the internal magnetic moments have been spontaneously aligned to the previous direction, we will find the phenomenon of hysteresis phenomenon. **Fig. 2.5** shows the curve of the hysteresis phenomenon. **Fig .2.6** integrates these three types of magnetism.

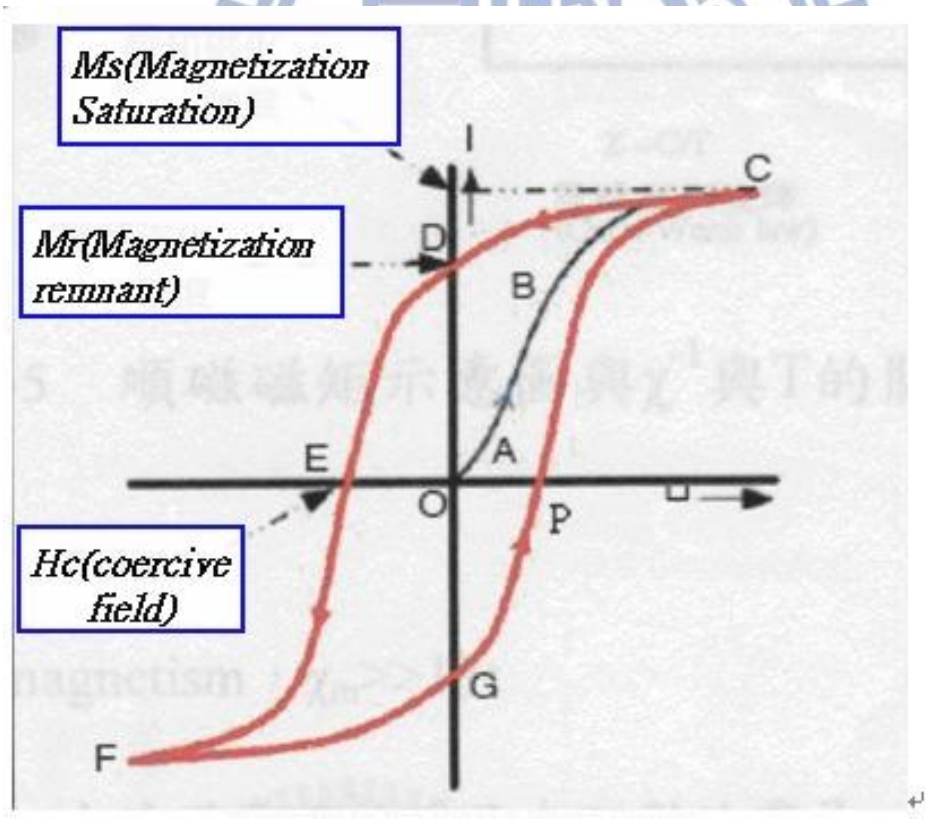

Fig. 2.5 Hysteresis curve of ferromagnetic materials.

Normally speaking, if the material shows the characteristic of the curve from A->B->C->D->E->F->G->P->C, it is ferromagnetic material.

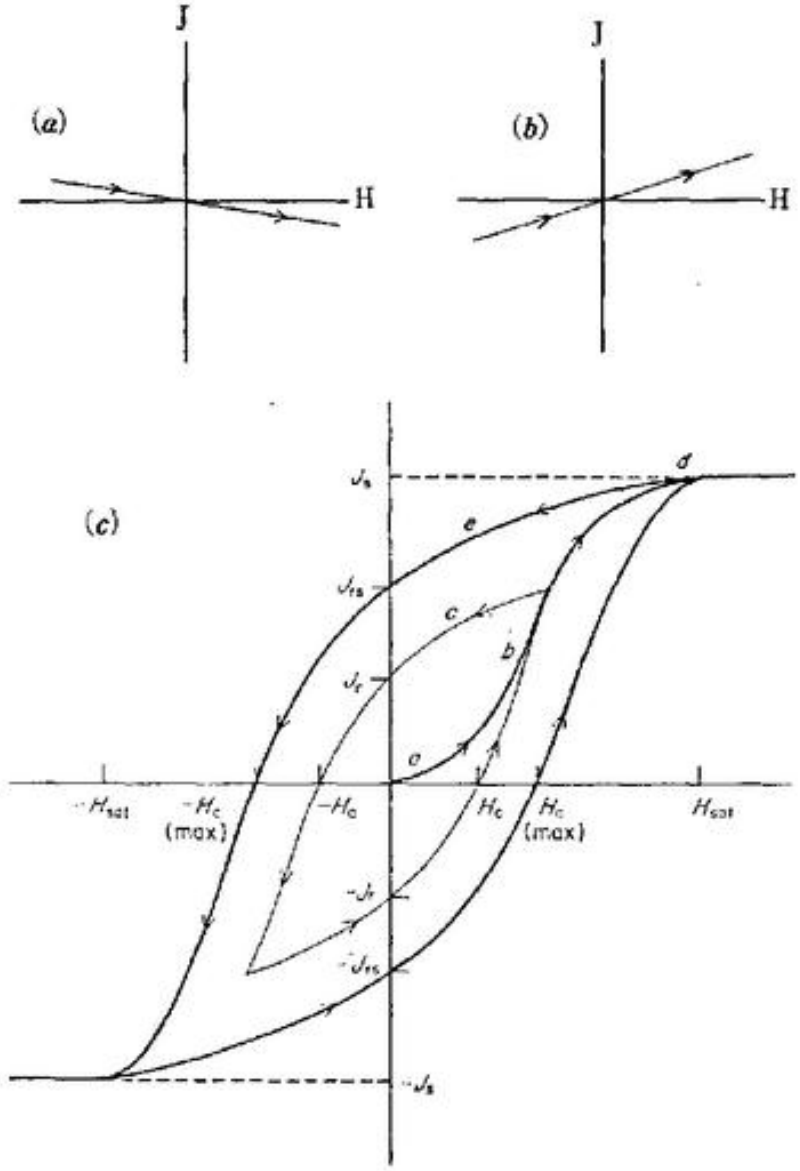

Fig. 2.6 (a) Diamagnetism (b) Paramagnetism (c) Ferromagnetism.

(4) Antiferromagnetism:

This type of materials has anti-parallel magnetic moments of the same amount, under macroscopic concepts, the sum of all magnetic moments is zero and if we applied a strong magnetic field, it will only show weak magnetism.

(5) Ferrimagnetism:

The internal structure of magnetic moments is similar to antiferromagnetic materials, it just does not equal the amount of magnetic moments in the opposite direction. Normally speaking, we can regard it as antiferromagnetic materials with less magnetic moment.

Fig. 2.7 shows ordered arrangements in electron spins.

Fig. 2.8 shows the schematic illustration of ferromagnetism.

Fig. 2.9 is summary schematic illustration of various magnetisms.

Fig. 2.7 Ordered arrangements in electron spins.

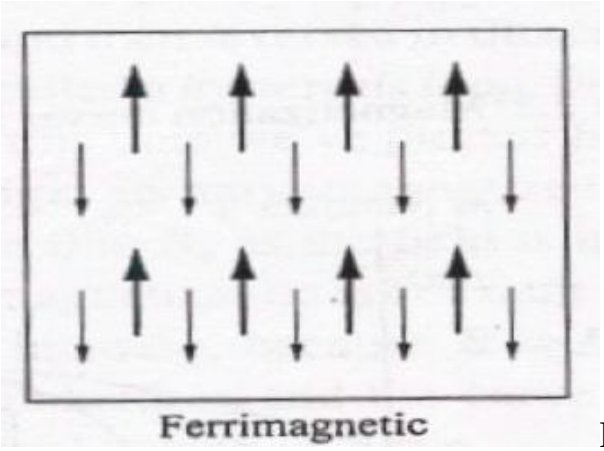

Fig. 2.8 Ferrimagnetism

To summary:

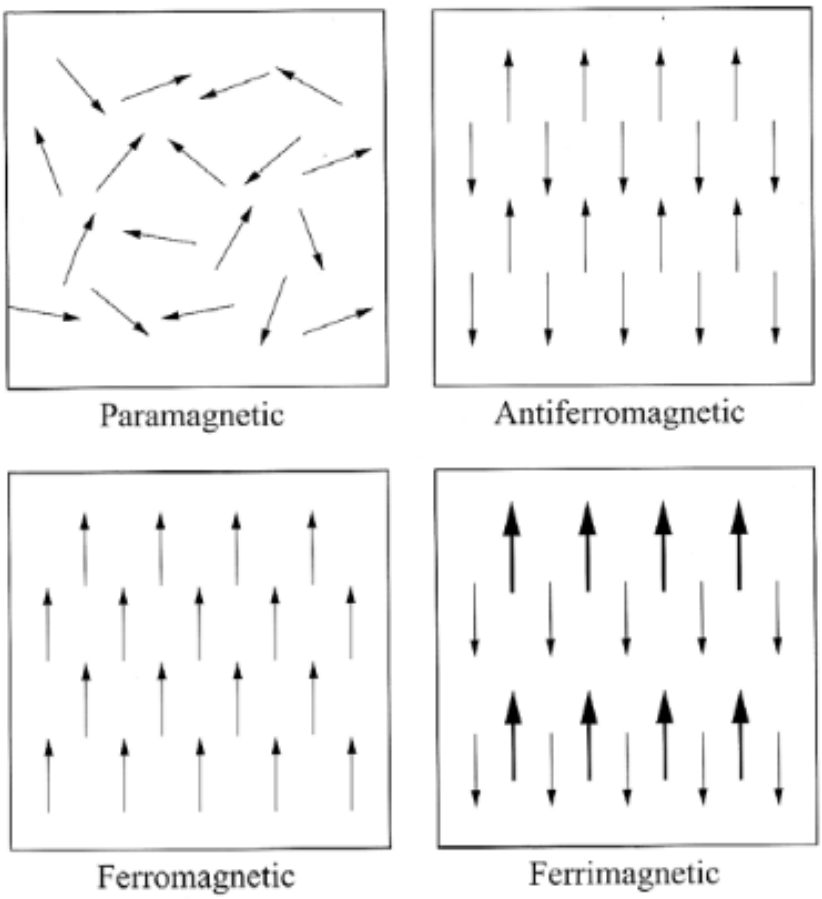

Fig. 2.9 Ordering of magnetic dipoles in a various of magnetic materials.

2-3 The mechanism and source of magnetism in DMSs

What's source of magnetism?

In 1907, PE Weiss's molecular field hypothesis was proposed, it was the first time to successfully establish a physical model of magnetism.
The Heisenberg model with molecular hydrogen in local magnetic systems lead to spontaneous magnetic moments interaction orderly, the result can attributed to quantum mechanics for exchange.
The model of Heisenberg exchange interaction successfully explains the first spontaneous magnetization phenomenon. Namely it plays a decisive role in the development of magnetic theories. Since then, the spontaneous magnetic theories had developed into two branches, "Molecular field theory" and "Exchange interaction theory". Exchange interaction theory is also divided into two models, the "Localized carrier theory" and "Itinerant carrier theory" **[53].**

Molecular field theory:

In order to explain the magnetization of ferromagnetic materials and magnetic characteristics, PE Weiss purposed two basic assumptions:

Molecular field hypothesis:

Ferromagnetic materials have the spontaneous magnetization below Curie temperature, leading to a molecular field about the size of 10^9[A ・ m^{-1}].
In the molecular field, atomic magnetic moments all align spontaneously. It confirms the assumption that the disorder effects which overcome thermal motion is not due to external magnetic fields but due to the molecular field.

Magnetic domain hypothesis:

Spontaneous magnetization is distributed by region, each magnetized region is called a magnetic domain, but the direction of spontaneous magnetizations are not same with magnetic domains, so the total macroscopic magnetic moment is zero. That is to say when materials are applied with a magnetic field, it can demonstrate a variety of macroscopic magnetic behavior by the variance of magnetic domains and the direction of spontaneous magnetizations.

Besides, if the temperature continuously increases, the kinetic energy due to thermal motion of magnetic moments will increase as temperature increases, then the spontaneous magnetization will be destroyed and ferromagnetism will transfer into paramagnetism when the sum of magnetic moments is large enough to compete with the molecular field. Although the characteristic of molecular field model is ferromagnetic in the earliest theoretical description, it has not explained completely why the volume magnetic moments have such a special relation with the molecular field. Therefore, researchers tried to find other models to elaborate it and proposed the model of exchange interaction theory which can be divided into two models: the “Localized carrier theory" and“Itinerant carrier theory” **[54].**

(1) Localized Carrier theory:

When magnetic atoms are doped into the semiconductors, it will supply the electron carriers (donors) and hole carriers (acceptors), and these produced carriers will be bound to the outer layer of the magnetic atoms. Because magnetic atoms themselves have spin waves in the outside layer

of the atom, these spin waves will affect the doping and make doping carriers have the same spin direction with spin carriers, when the two spins overlap each other, those magnetic atoms achieve spin-spin coupling interaction through interaction of bound magnetic carriers, as **Fig. 2.10 shows.**

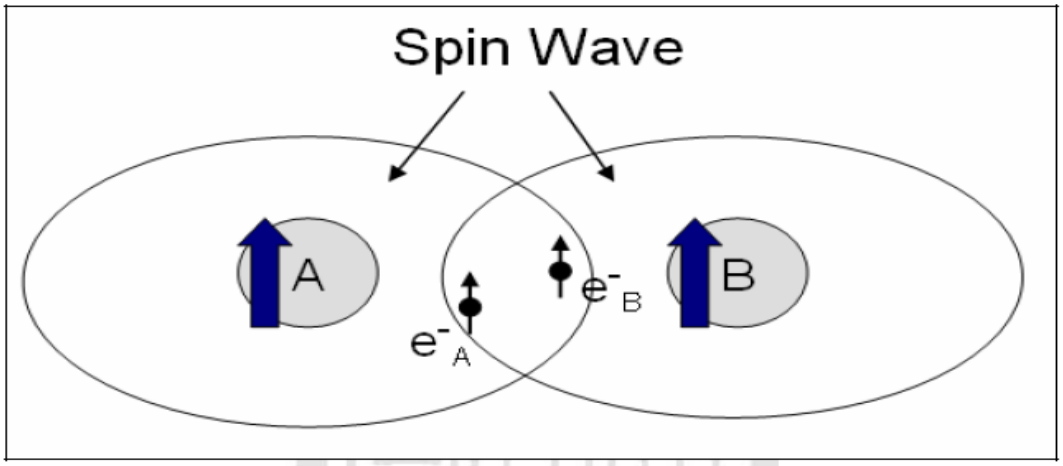

Fig. 2.10 The model of localized carrier theory.

(2) Itinerant carrier theory:

When magnetic atoms are doped into the semiconductors, these produced carriers will not be limited to being around magnetic atoms, but in the form of free carriers. After interactions between the produced and induces carriers, they will have the same spin signal and thus contribute to magnetism, such as **Fig. 2.11.**

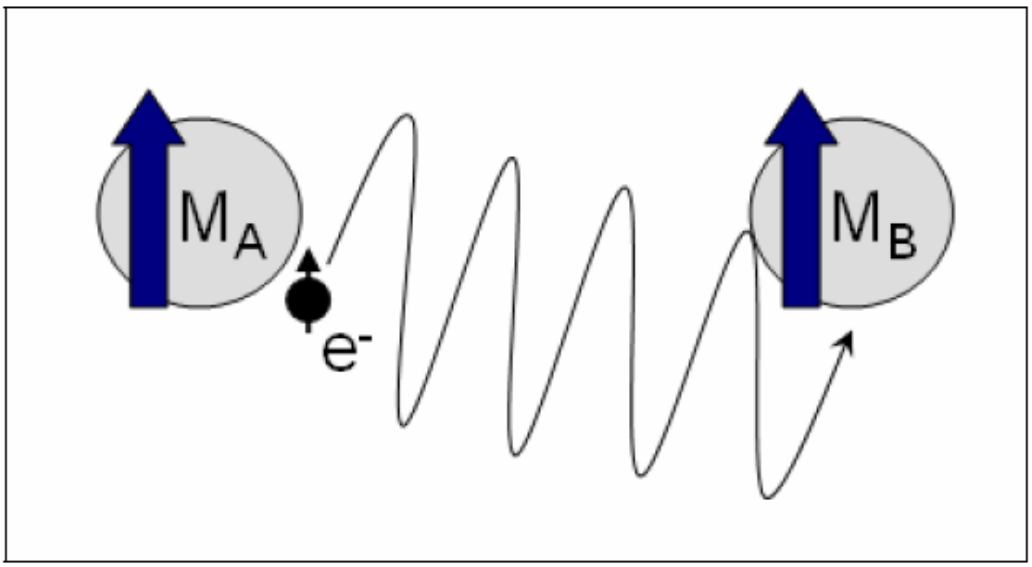

Fig. 2.11 The model of itinerant carrier theory.

As mentioned above, because the two models can't explain the variance and source of magnetism of DMS, some researchers propose different models to explain the source of magnetism more carefully. Such as Bound magnetic polaron (BMP) 、Exchange interaction (Direct exchange、Double exchange、Super exchange) . We will introduce these models in the following.

2-3.1 Bound magnetic polaron (BMP)

In 2004, JMD Coey's research team purposed the Bound magnetic polaron (BMP).The model of BMP can be expressed using **Fig. 2.12.** For a simplified description, small hollow circles represent atom of Zinc, these circles which are black and small represent doped magnetic atoms, and hollow squares represent oxygen vacancies. The direction of arrows are the direction of magnetic moments, the black shadows are bounded by excess electrons caused by oxygen vacancies. They believe that when one oxygen atom leaves, an oxygen vacancy will form and will produce a unit positively charged oxygen vacancy and the original electrons bounded by Zns and Oxygens becomes free electrons due to generation of oxygen vacancies.

However, because there were positive charges of oxygen vacancies, it attracts electrons and makes them lose their freedom, so we call it bound electrons or magnetic polarons. In the regions of squares, if there are magnetic atoms, it will cause interaction of spin magnetic moments and make all the magnetic moments align the same direction, causing ferromagnetic coupling and make materials show ferromagnetism.

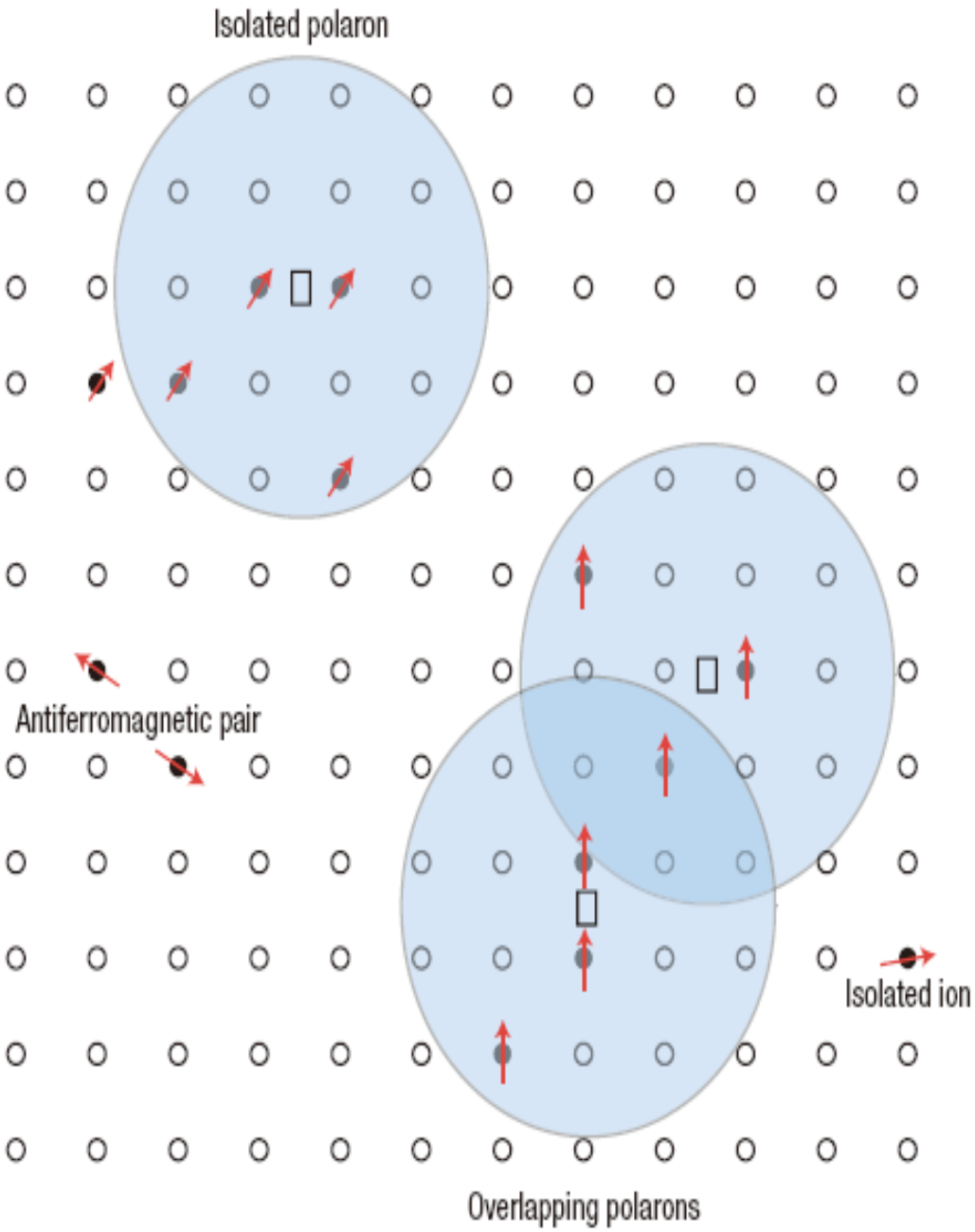

Fig. 2.12 BMP Model

Cation sites are represented by small circles.

The unoccupied oxygen sites are represented by squares.

2-3.2 Mechanism of exchange interaction

Direct exchange:

If electrons on neighboring magnetic atoms interact with an exchange interaction, this is known as “direct exchange”. This is because the interaction proceeds directly without any intermediate progress. Despite it being the most obvious exchange interaction, this situation seldom occurs. That is to say that direct exchange is not the most important mechanism of magnetic properties.

Double exchange:

It was purposed originally by Clarence Zener who explains how electrons exchange between two species and why materials become ferromagnetism. In some oxides, it’s possible that the magnetic atoms show mixed valence, namely magnetic atoms can exist more than one oxidation state. Take some compounds for instance, in Manganese (Mn) oxide materials, Mn ion which can exist in oxidation state Mn^{3+} or Mn^{4+}, such as **Fig. 2.13** shows. Besides, these situation often occur in Colossal magnetoresistance materials, such as $La_{1-x}X_xMnO_3$ material, “X” represents “Ca”, ” Ce” and so on. When “X” is “Ca”, because “Ca” is normally two valence, therefore Mn will become the mixed valence of Mn^{3+} or Mn^{4+}. Relatively, when “X” is “Ce”, because “Ce” is normally four valence, Mn will then become mixed valence of Mn^{3+} or Mn^{2+}. Such behavior causes $\underline{e_g}$ electrons on a Mn^{3+} ion can hop to a neighboring site when there is a vacancy of the same spin, if its neighbor is a Mn^{4+} which has no electrons on its e_g shell. The e_g electron on a Mn^{3+} ion can hop to a

neighboring site only if there is a vacancy of the same spin. If the neighbor is a Mn^{4+} which has no electrons on the e_g shell, this should present no problem. However, there is a strong single-central exchange interaction between the e_g electron and the three electrons in the t_{2g} level which wants to keep them all aligned. To our knowledge, it is necessary to maintain the characteristic of high spin hopping if we want to get ferromagnetic alignment. As a result, the ability to hop saves kinetic energy which in turn, as shown in **Fig. 2.13(a)** reduces the overall energy. Besides, it is not favorable for an e_g electron to hop to a neighboring ion in which the t_{2g} spins will be antiparallel to the e_g electron as **Fig. 2.13(b)**.

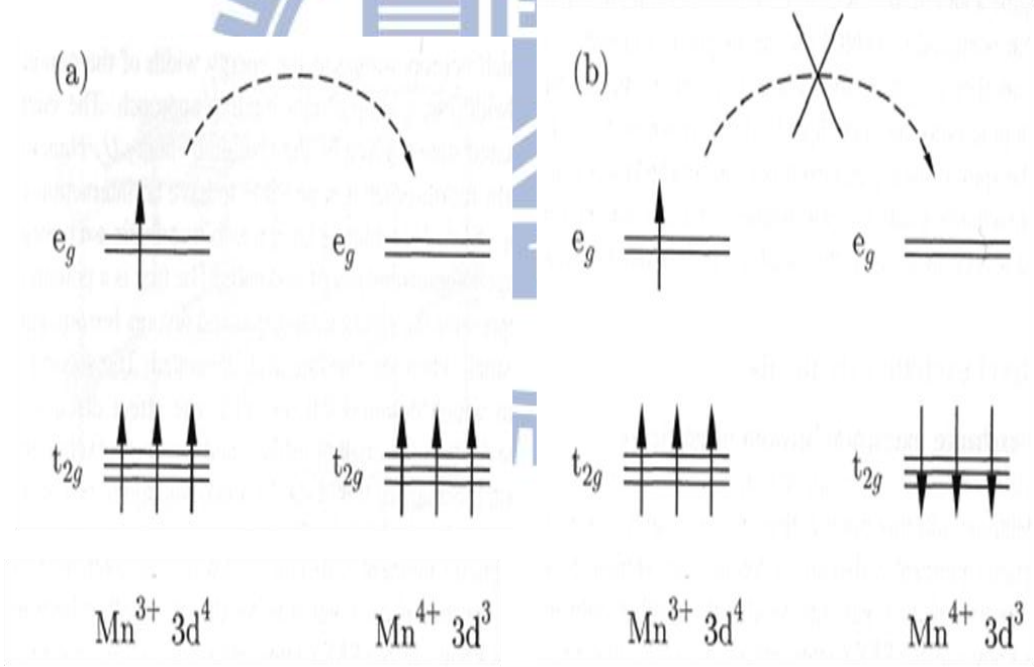

Fig. 2.13 Schematic that depicts the hoping processes in double exchange.

Super exchange:

Super exchange is an indirect interaction caused by the virtual hopping of electrons among the non-neighboring magnetic ions because of adding excess oxygen ions. **Fig 2.14(a)** shows two transition metal ions separated by an oxygen ion. To our knowledge, every transition metal ion has unpaired electrons in the d orbital, and the oxygen has unpaired electrons in the p orbital, the overlap of unpaired electrons in d and p orbitals causes p-d hybridization. The electrons on the left side of the oxygen p orbital could migrate to the neighboring transition metal. The remaining electron in the oxygen p orbital can be paired with the other neighboring transition metal. According to the Pauli exclusion principle, electrons in transition metals become antiparallel to the mediating one. Therefore, it causes antiferromagnetism.

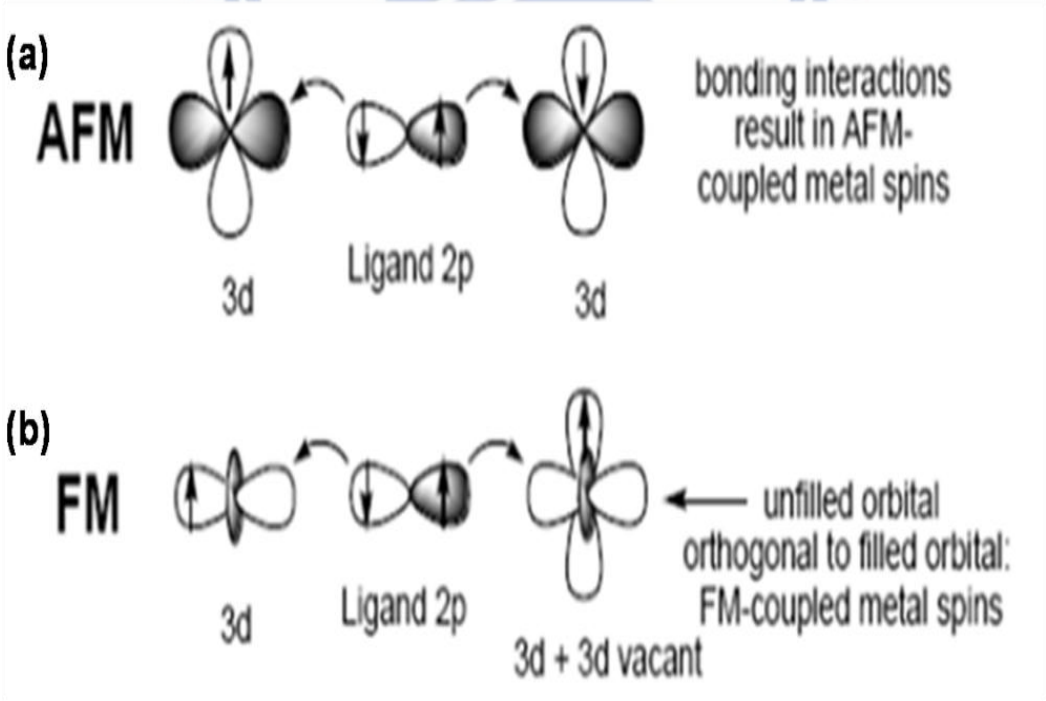

Fig. 2.14 Schematics depicting the hopping processes in super exchange and double exchange.

To summarize of exchange interaction as **Fig. 2.15**.

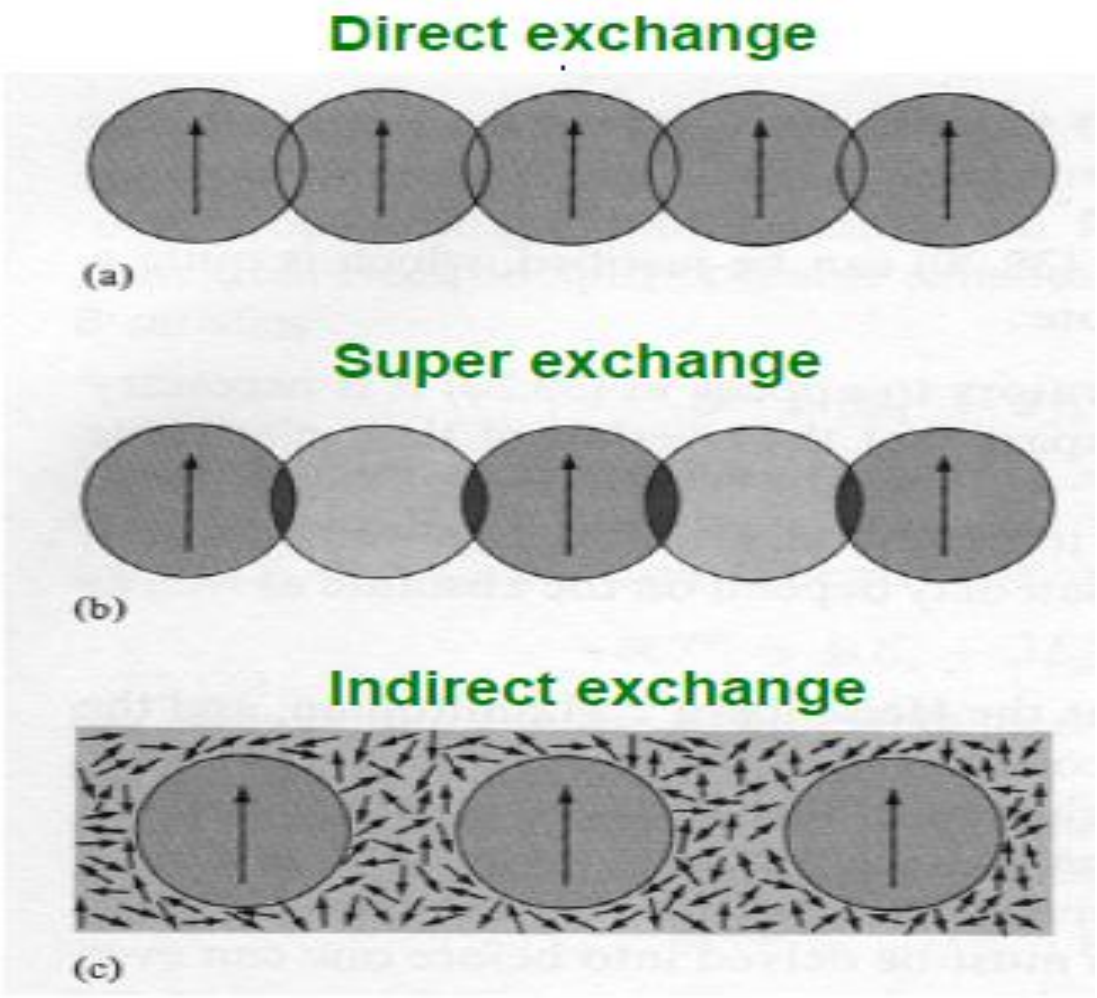

Fig. 2.15 Schematics of **(a) direct exchange**

(b) super exchange (c) indirect exchange.

Chapter 3

Experiments and Instruments

3-1 Sample preparation

Because we want to get the different ratio of carbon doping concentrations, we make three samples of different carbon doping concentrations in the beginning. The three samples are of 0%, 2%, and 5% carbon doping concentration respectively.

3-1.1 Target fabrication

In the first, we use high purity rutile titanium dioxide (99.98%) to mix with the carbon powders (99.999%) for the purpose of getting the carbon-doped TiO_2 mixture, and we use the agate bowl to stir the two kinds of powder for the purpose of making them as uniform as possible. Second, we utilized the heater to heated the mixture from room temperature 27^{o}C to high temperature 1200^{o}C for 24hours. This step is to make the mixture more uniform, namely increase the contact area between carbon and TiO_2 powders to ensure the well mixing. Third, we utilized the gas pressure machine to press the mixture and sinter it at 1200 ^{o}C for 24 hours.

PS: For the purpose of promoting reactions among these mixed constituents, we may grind the target body into powder and repeat the second and third step. Then we can get a target body, and our next step is to use Pulse Laser Deposition (PLD) to make the target become thin film by implementing below procedures.

3-1.2 Pulsed laser deposition (PLD)

During PLD, a high energy laser pulse is focused on the surface of our target body. After it absorbs the strong electromagnetic radiation, local areas of the target body is instantaneously vaporized to form plasma which would be deposited on the substrate. For the purpose of getting thin films with ferromagnetism, we have tried to make various deposition conditions. These films were grown by the 248nm KrF excimer laser with laser engrey density $2J/cm^2$, repetition rate 5Hz, temperature of substrate change from room temperature to 600^oC, oxygen pressure change from 0.02torr to 0.2torr.

Following is the procedures for preparing carbon-doped TiO_2 thin films:

1: Clean the substrate with Acetone (ACE), Methanol, and DI Water under the ultrasonic vibration for ten minutes respectively.

2: Dry and clean the substrate with nitrogen gas gun.

3: Stick the substrate on the stainless steel plate by silver paste.

4: Turn on the laser light source to confirm whether the laser focus on the center of the target.

5: Heat the plate to 150 ^oC to make silver paste become solidified so that the substrate can be fixed on the steel plate.

6: Put the plate in chamber of our PLD system with thermal couple imbedded.

7: Pump the chamber till the base pressure is lower than 10^{-6} torr for one hour at least.

8: Heat the substrate to the preset temperature.

9: Set the power energy and the repetition rate of the excimer pulsed

laser.

10: Control the partial oxygen pressure to our expectation

11: Turn on the excimer laser and calculate how much time we have to pump our target with a timer.

12: Quench the substrate to room temperature after completing our above procedures by filling the chamber with oxygen, this step is to equilibrate the chamber's pressure with our atmosphere.

13: Take out the sample.

3-2 Structure analysis by XRD

Introduction of X-ray diffraction

X-ray diffraction is a popular technique for investigating crystal structures. It is based on constructive interference between monochromatic X-rays and crystalline samples. The interaction of incident rays with the samples produce constructive interference when conditions satisfy Bragg's Law ($2d \sin\theta = n\lambda$) **(Fig. 3.1)**. The "d(Atomic Spacing)" represents the distance between the two parallel planes, "θ" is the angle between the incident X-Ray light and the lattice surface, "n" is an integer(Normally we set it to "one" here), and "λ" is the wavelength of the incident X-Ray light. In our experiment instrument, Cu Kα"λ"is 0.154056 nanometer (Nm), the diffracted X-rays are then detected by the detector which can scan the angle (2θ) from 0^o to 90^o. Then, we can compare the Intensity-2θ graph to the original data base, to confirm whether there exists the other impurity phases.

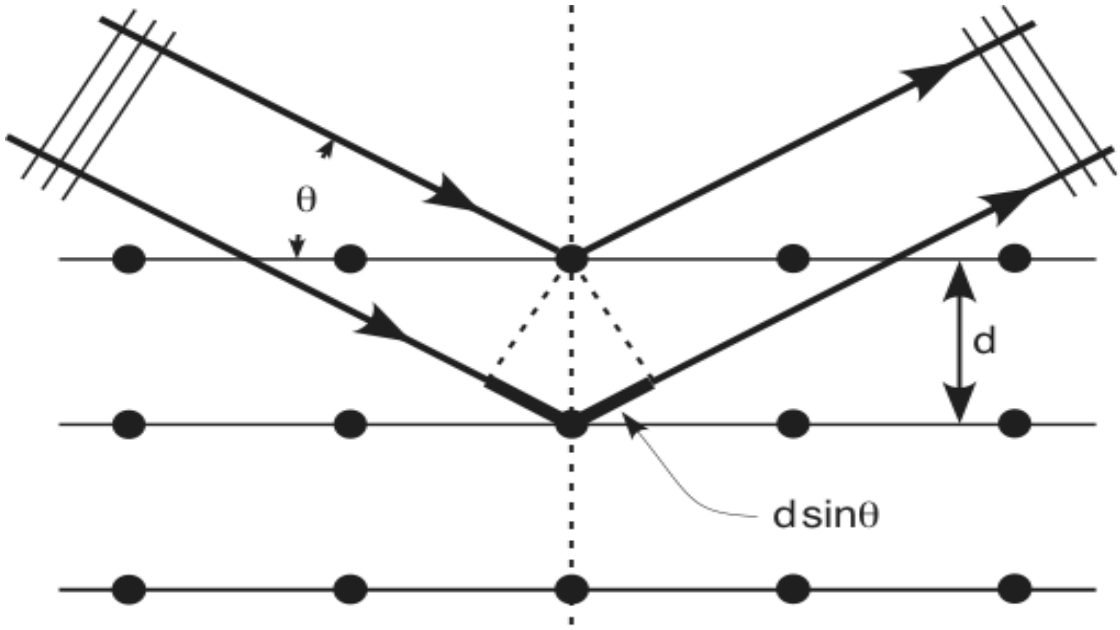

Fig. 3.1 Illustration of XRD process.

3-3 Analysis of magnetism

3-3.1 Introduction of the Superconducting quantum interference device (SQUID)

Superconducting quantum interference device (SQUID) (**Fig. 3.2)** is a delicate equipment which measures magnetization versus temperature (M-T) or magnetization due to magnetic field (M-H). Moreover, it incorporates the characteristics of electronics, low temperature, and high vacuum techniques.

When we talk about intrinsic structure of SQUID, it is mainly composed of the two parallel Josephson junctions connecting two superconductors separated by a thin (about ~1nm) insulating layer.

When the magnetic flux is varied as bias currents, it causes oscillation of voltage, then the equipment can reads the variance of magnetic field by

change of voltage. Therefore, it can detect the small magnetic fields and measure the extremely weak magnetic signals. Sensitivity of SQUID is about 10^{-8}emu with 0.1T external magnetic field applied, temperature of measurement can range from 2K to 800K, the magnetic field can range from -7 Tesla to 7 Tesla (-70000Oe to 70000Oe). We can make the most of the delicate equipment (SQUID) to measure the M-H and M-T curve, to understand the relationship between magnetization and temperature (or magnetic field). It is helpful and essential for our studies.

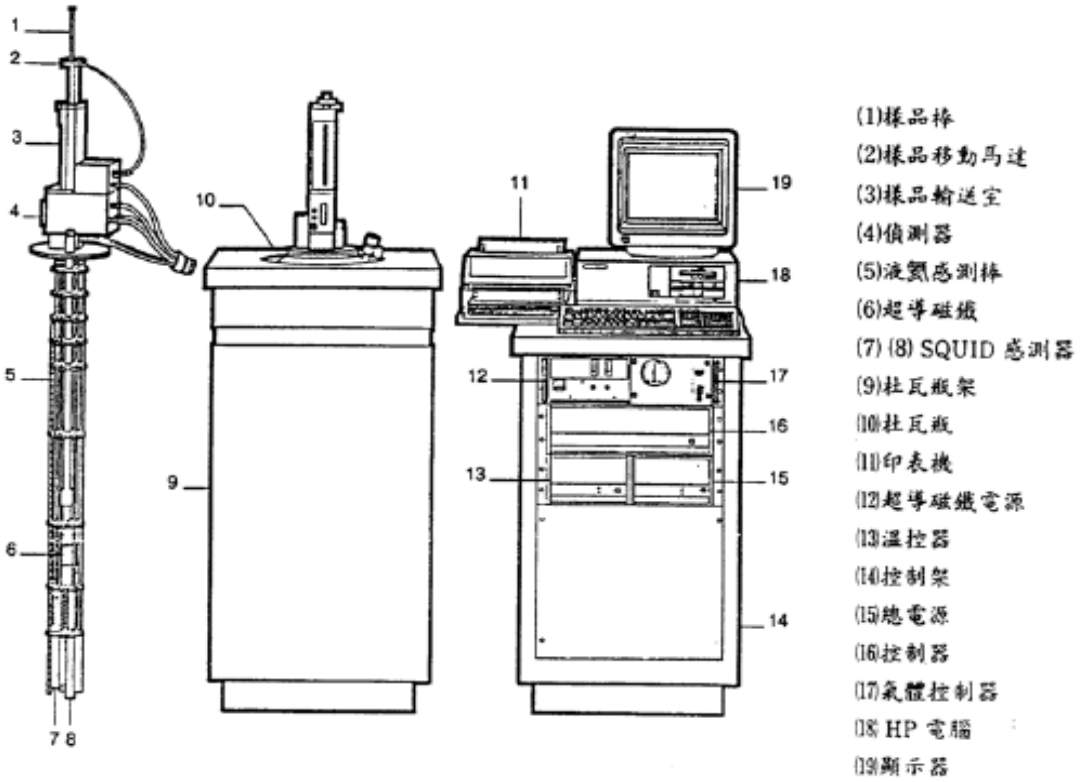

Fig. 3.2 Schematic illustration of SQUID

3-3.2 The principle of Josephson junctions

(Josephson effect and Josephson junctions)

Josephson interface **(Fig. 3.3)** is sandwiched between two superconducting materials and a thin (~ 1nm) insulating layer which inserted to form the barrier energy, superconducting electrons can pass through this layer and form superconducting currents.

Josephson junction equivalent circuit **(Fig. 3.4)** can be simulated, the total flow through the Josephson junction current "I" is generated by the capacitive displacement current, normal current(In), and Josephine current(Is).When the Cooper electron pairs in the form of a non-resistive superconductor tunneling from the superconductor to the other side of the insulation process, we call it DC Josephson effect.

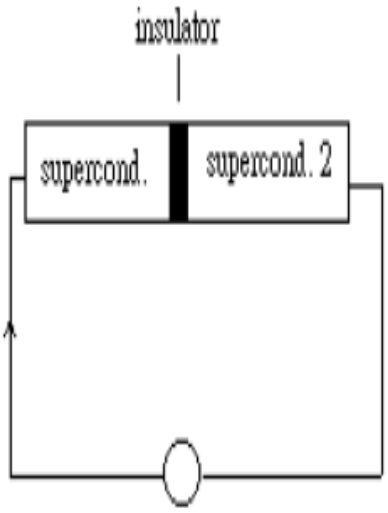

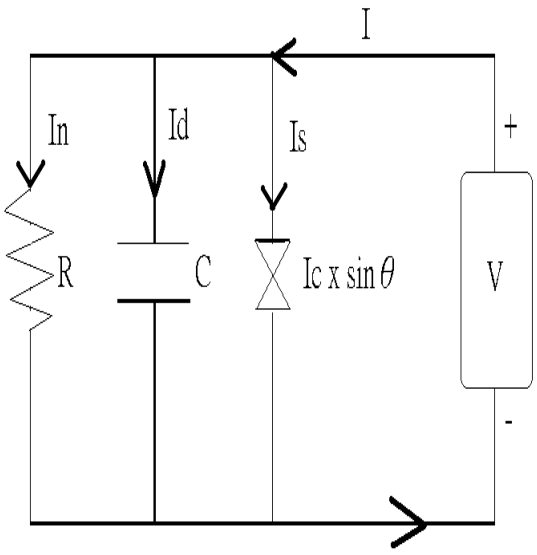

Fig. 3.3 Josephson junctions

Fig. 3.4 Josephson Circuit

3-4 Surface electronic structure analysis

3-4.1 What's X-ray Photoelectron Spectroscopy?

X-ray Photoelectron Spectroscopy (XPS), also called Electron Spectroscopy for Chemical Analysis (ESCA), is a common technique of surface element analysis. It can not only detect the elemental composition, but also detect the chemical bonding among elements by observing the Intensity-Binding energy (eV) graph. The principle of XPS is based on the photoelectronic effect, which produces monochromatic X-rays to irradiate the substance, and excites out electrons from atoms. Namely the sample would emit electrons after being irradiated by a photon source with enough energy **(Fig. 3.5)**. We can realize conditions of surface and bonding by observing the distribution of photoelectron energy.

When it comes to the photoelectronic effect, we have learned the phenomenon in senior high, we can calculate the electron binding energy by the equation based on the work of Ernest Rutherford:

$$E_{binding} = E_{photon} - E_{kinetic} - \Phi$$

where $E_{binding}$ is the energy of electrons emitted from one electron configuration within the atoms, E_{photon} is the energy of the x-ray photons being used, $E_{kinetic}$ is the energy of emitting electrons as measured by the instrument and Φ is work function of the spectrometer.

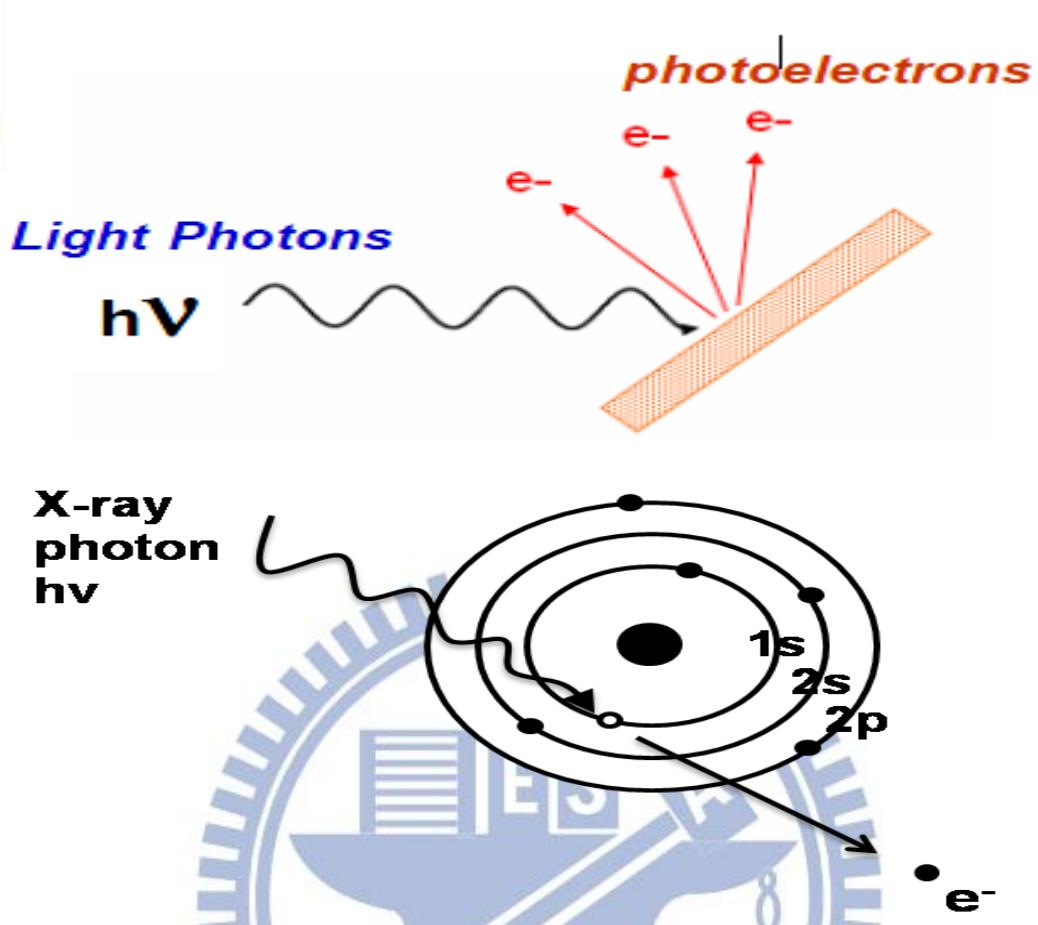

Fig. 3.5 X-ray Photoelectron Spectroscopy **(XPS).**

3-4.2 Chemical state identification

As mentioned above, we can calculate binding energy by measuring the kinetic energy of the photoelectrons, further we use intensity-binding energy graph to judge elemental and chemical states of valence electrons. Owing to valence electron bondings, atoms in the compound produce the phenomenon of interactive electron transport. Therefore, the electrons don't show neutral characteristics, the inner electrons are affected by the electrostatic force field, and cause changes in energy levels and binding energy of photoelectrons. It's called "Chemical Shifting".

In conclusion, XPS provides a tool to identify individual chemical state of an element, namely we can detect the chemical bonding by XPS. As the oxidation state changes, the core level peaks also change original position and cause peaks shift. Normally speaking, if the chemical reaction causes the higher oxidation state of elements, these elements would exhibit higher binding energy and vice versa. After the original peaks shift, we can get the information of new chemical bonding among elements.

3-5 X-ray absorption near edge structure (XANES)

What's X-ray absorption near edge structure (XANES)?

X-ray absorption near edge structure (XANES), also known as Near edge X-ray absorption fine structure (NEXAFS) which is a type of absorption spectroscopy, it indicates the absorption peaks due to the photo absorption cross section in the X-ray absorption spectra (XAS) observed in the energy region.

What's the difference between XPS and XANES?

The most obvious difference between XANES and XPS is that the XPS only can probe the **occupied state** below the Fermi level. However, the XANES only can probe the **unoccupied** state of materials, the transitions To bound vacant states above the Fermi level can be seen.

The principle of XANES：

When it comes to the spectrum of XANES, we can summarize two methods: "X ray fluorescence yield" and "Total electron yield".
When X-ray irradiates the sample, it will excite the photoelectron to move toward the surface. Because of the limitation on mean free path of the electrons, it's more difficult for the deeper electrons to reach continuum states, therefore the total electron yield is a more appropriate method to investigate the surface characteristics of samples.

On the other words, electrons will leave empty orbits after X ray excites out the photoelectrons, these empty orbits will be occupied by higher level electrons which emit photons and produce fluorescence.

As Fig. 3.6 shows, when the X-ray hits a sample, the oscillating electric field of the electromagnetic radiation interacts with the electrons bound in an atom. Either the radiation will be scattered by these electrons, or absorbed and excite the electrons.

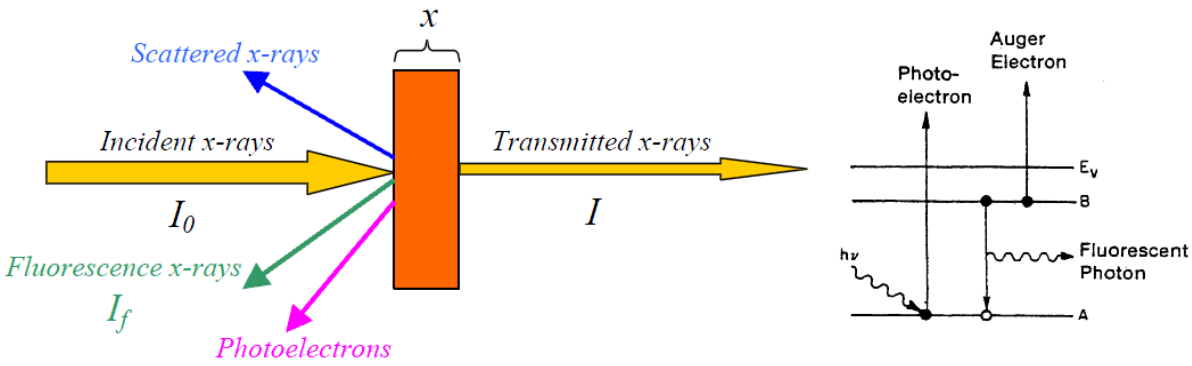

Fig. 3.6 Schematic illustration of XANES.

Why are we interested in XANES?

XANES can be described qualitatively in terms of **coordination chemistry** that includes regular, distorted octahedral and tetrahedral; **molecular orbitals** that includes p-d hybridization, p-p coupling, crystal field theory; **band structure** that includes the available density of occupied electronic states, **multiple scattering** that includes multiple bounces of the photoelectrons. Above the explanations about physics and chemistry all have the relation with what's electronic state and how the photoelectrons fill the orbitals.

The advantages of XANES

The great advantage of XANES derives from its elemental specificity. Because the various elements have different core level energies, XANES permits extraction of the signal from a surface monolayer or even a single buried layer in the presence of a huge background signal. On the other hand, XANES also has the function to determine the chemical state of many elements which are present in the different places in the material, we can get a variety of information by investigating the change of chemical properties, and the most important property to us is that XANES can be done at lower doping concentrations, and less than perfect sample conditions, it is indispensable for my low doping carbon concentration experiment.

What's the contribution of XANES to our experiment?

We utilize XANES to investigate the change of oxidation state and valence electrons for the purpose of confirming whether the carbon doping is actually mixed with the titanium dioxide. If the main edge of photon energy shifts to higher energy with increasing oxidation state, it represents the fact that the carbon actually entered into the system of carbon-doped TiO_2.

Chapter 4

Results and discussion

4-1 The characteristics of carbon-doped TiO_2 powders

4-1.1 Structure analysis of powders by XRD

In the beginning, for the purpose of investigating the effect of different carbon concentrations, we make three kinds of powders respectively, it were pure titanium dioxide, 2% carbon-doped titanium dioxide, and 5% carbon-doped titanium dioxide. After we make the three kinds of samples, we utilize XRD to analyze structure; it is obvious that it presents the rutile phase **(See Fig. 4.1)** which matches the result that titanium dioxide has the trend to become rutile at high temperature. What's more, we get the carbon signal although it's weak. On the basis of our inference, it is possibly a result of too low concentration of carbon doping which explains why seldom people do research with low concentration of carbon doping. Nevertheless, we think it is interesting to understand what's the effect of rare concentration of carbon doping.

.

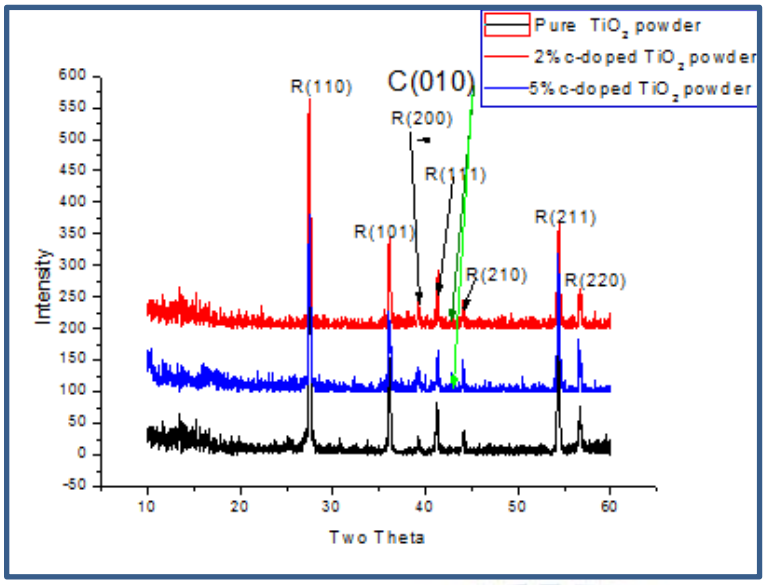

Fig. 4.1 The XRD of initial three kinds of powders.

4-1.2 Magnetic analysis of powders by SQUID

After we analyze the XRD, we clearly know our phase is rutile. But it is still a suspicion of whether the carbon doping affects the titanium dioxide system. Therefore, we use the superconducting quantum interference device (SQUID) to measure M-H curve of the three kinds of powders, and get result **(as Fig.4.2)**, the powders of pure titanium dioxide are paramagnetic, but the powders of carbon-doped titanium are ferromagnetic, it is consistent with previous experiments that it is possible to induce ferromagnetism in TiO_2 system through carbon doping. However, there are small differences between 2% and 5% carbon doping, therefore we maintain doubtful of the result, whether the effect of carbon doping reach saturation between 2% and 5% doping.

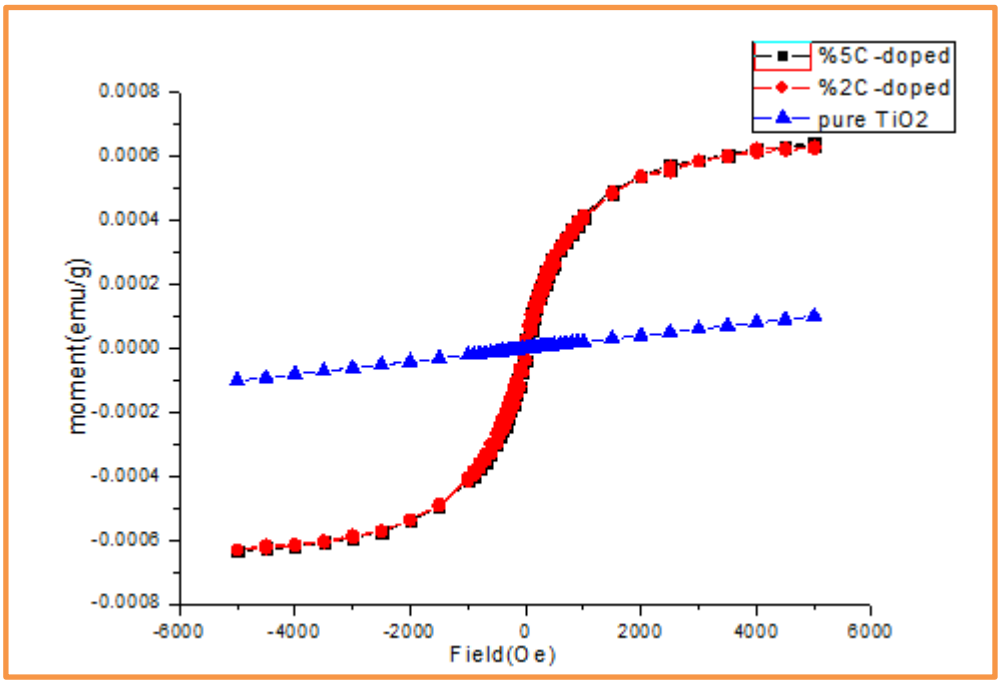

Fig. 4.2 The M-H curves of the three kinds of powders.

Because most of the studies of carbon-doped TiO_2 is about photocatalyst, which especially focuses on using powders, seldom people conduct research on the characteristics of magnetism of carbon-doped TiO_2 which exist in state of thin films, thus, we decided to do research mainly using thin films.

We used our pulse laser deposition (PLD) system to make the bulk become thin film under different temperatures and oxygen pressures in order to realize the magnetic mechanism in thin film system. Whether the powder and thin films have similar structures and magnetic behavior, and what's the reason for the differences.

After a series of growth situations, we tried to change the temperature and oxygen pressure, and use the $SrTiO_3$ as our substrate, for the purpose of discussing the doping, it is impossible to use too high temperature in our growth progress because it is possible to make the doping element out of carbon-doped TiO_2 system although the sample usually has more excellent crystal phases with temperature increases. Therefore, we choose $400\,^{o}C$ as the growth temperature. Besides, we also take oxygen pressure into consideration. Normally speaking, people prefer lower oxygen pressure in process of growth, but we want to know what'll happen in the contrary condition, namely, we use the situation of high oxygen pressure as our condition of growth.

4-2 The characteristics of carbon-doped TiO_2 thin films

4-2.1 Structure analysis of thin films by XRD

After we successfully get these thin films, we utilize XRD to analyze their structures for the first time, it is apparent that it undergoes phase transition from rutile to anatase **(Fig. 4.3 (a)-(d))**.

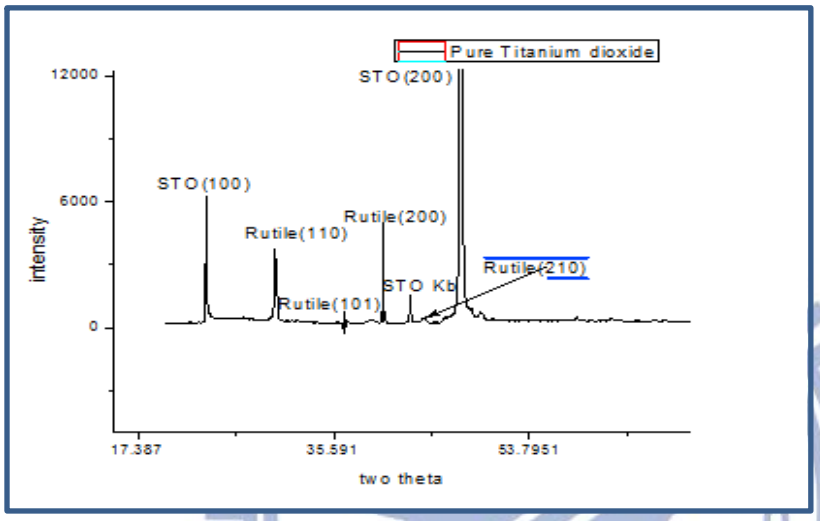

Fig. 4.3 (a) XRD of pure TiO_2 thin film at 400 ^{o}C and 0.2torr.

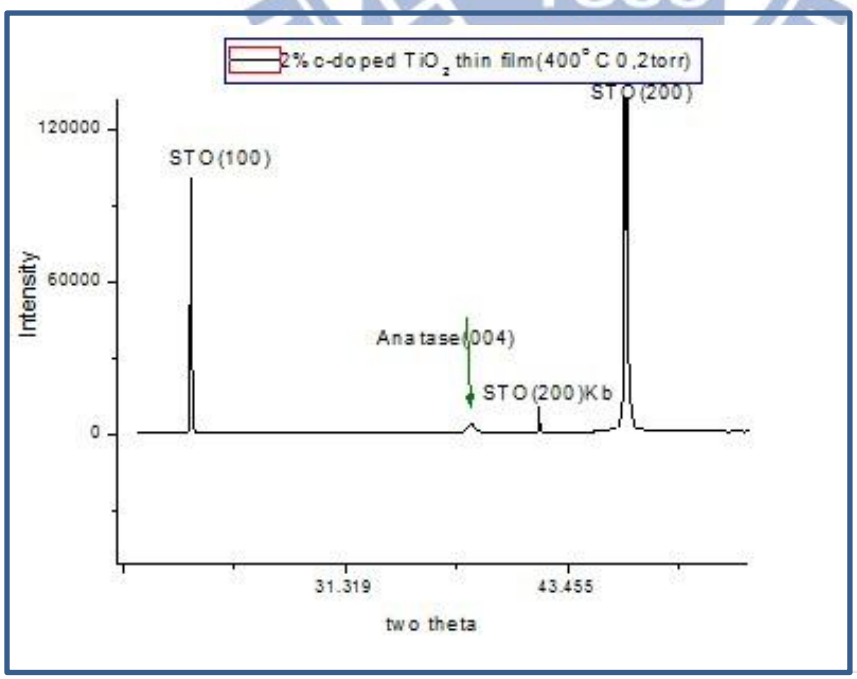

Fig. 4.3 (b) XRD of 2% C-doped TiO_2 thin film.

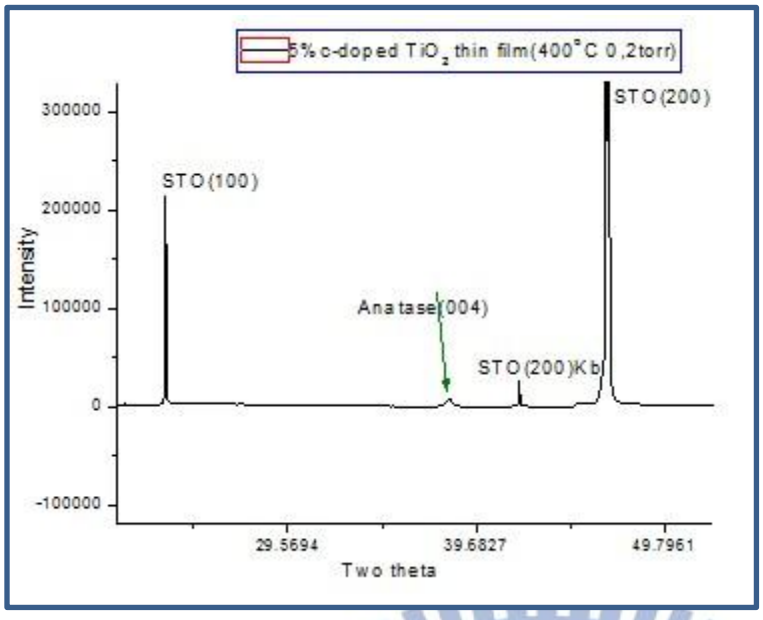

Fig. 4.3(c) XRD of 5% C -doped TiO_2 thin film.

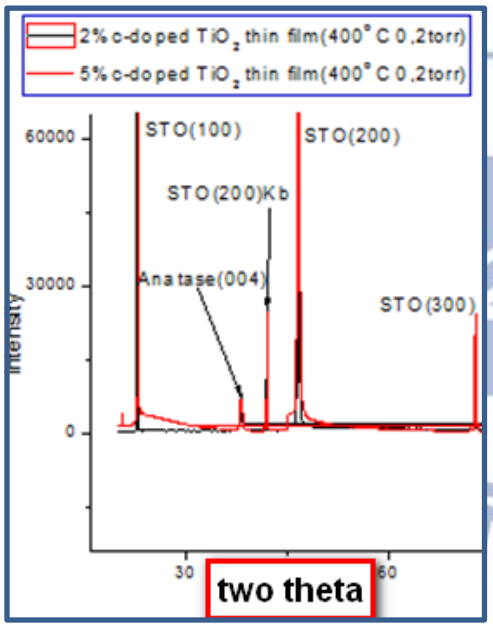

Fig. 4.3(d) The comparison of XRD of pure, 2% C-doped, and 5% C-doped TiO_2 thin films.

Using XRD, we determined that powder and thin film might not have similar structure. Despite the phase change to anatase from the rutile phase, it is consistent that carbon-doped titanium dioxide causes more stable anatase phase than rutile phase. To summarize, we get the anatase phase thin films of TiO_2.

4-2.2 Magnetic analysis of thin films by SQUID

After we confirm the structure of thin films, we dedicate to investigate whether different carbon concentrations have different effects on magnetism for the purpose of understanding characteristics of magnetism. Therefore, we used SQUID to measure the three kinds of powders and obtain the result as **Fig. 4.4.**

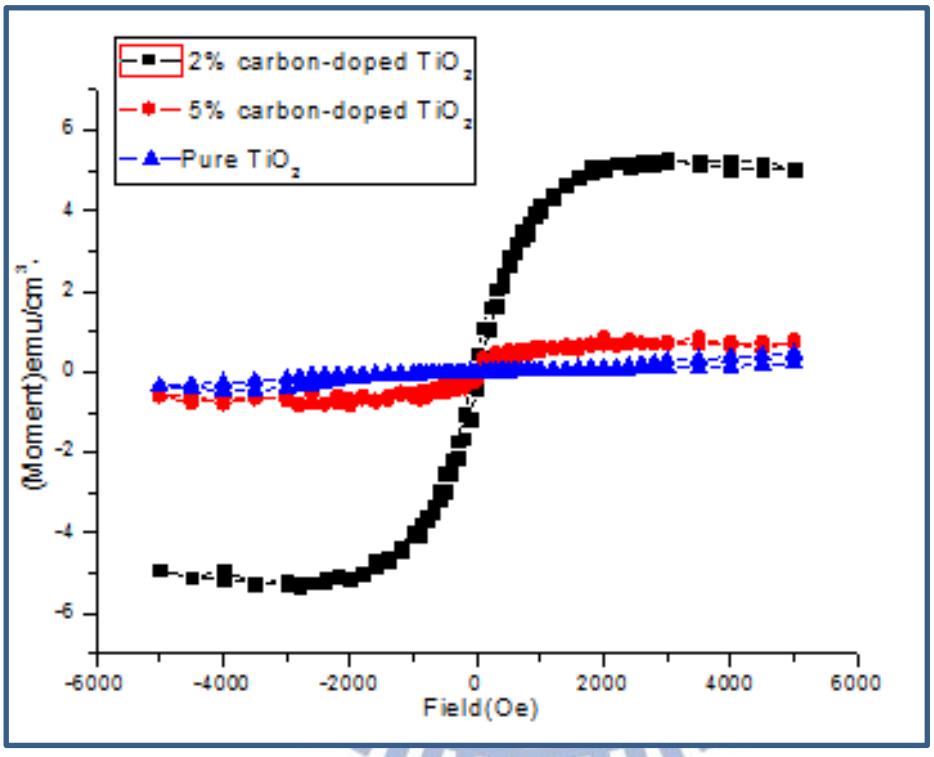

Fig. 4.4 The M-H curves of the three kinds of thin films.

We get absurdities from Fig. 4.4, why does the 2% carbon doped TiO_2 have higher volume in magnetic moment than 5% carbon doped TiO_2? What's happened in the progress? Does there exist some unknown bonding or excess carbon? For the purpose of solving these questions, we use XPS to investigate the surface electronic structure.

4-3 Surface electronic structure analysis by XPS

To our knowledge, there are three elements in the system of carbon-doped TiO_2, titanium, carbon, and oxygen. We utilize XPS to observe these samples and to analyze these elements. At first, we took advantage of XPS to analyze elements of titanium in pure, 2%, and 5% carbon-doped TiO_2 respectively, we can clearly observe the bonding of **TiC** in the 2%C-doped TiO_2 **(such as peak 0 in Fig. 4.6)** and in the 5%C-doped TiO_2 **(such as peak 0 in Fig. 4.7).**

On the other hand**,** pure TiO_2 has no **TiC** bonding **(such as Fig. 4.5),** these results are consistent with the fact that TiC bonding is the key to induce ferromagnetism.

We also confirm the conclusion that ferromagnetism can be induced by carbon doping. However, although the 2%, and 5% carbon-doped TiO_2 both form the TiC bonding, the 5% carbon-doped TiO_2 has less magnetic moment than 2% carbon-doped TiO_2. Therefore, we make an assumption that the excessive carbons cause extra effects so that the magnetic moment decreases with increasing carbon concentration, after we investigate the XPS of O 1s, we confirm that our assumption is correct because there are some carbon that aren't bonded in the system of 5% carbon-doped TiO_2 **(such as peak 2 in Fig. 4.13).**

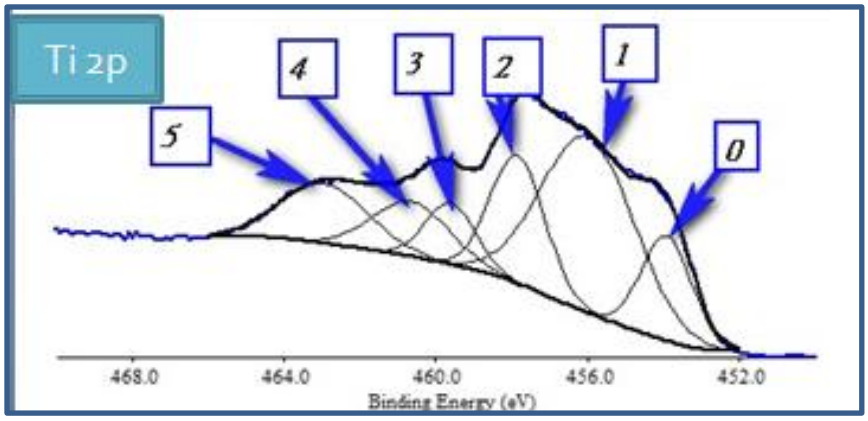

Fig. 4.5 XPS of Ti 2p (TiO_2 with 0% carbon).

Peak	Position (eV)	element or bonding
0	453.911	Ti $2p_{3/2}$
1	455.997	TiO $2p_{3/2}$
2	457.858	Ti_2O_3 $2p_{3/2}$
3	459.610	Ti $2p_{1/2}$
4	460.656	TiO $2p_{1/2}$
5	462.960	Ti_2O_3 $2p_{1/2}$

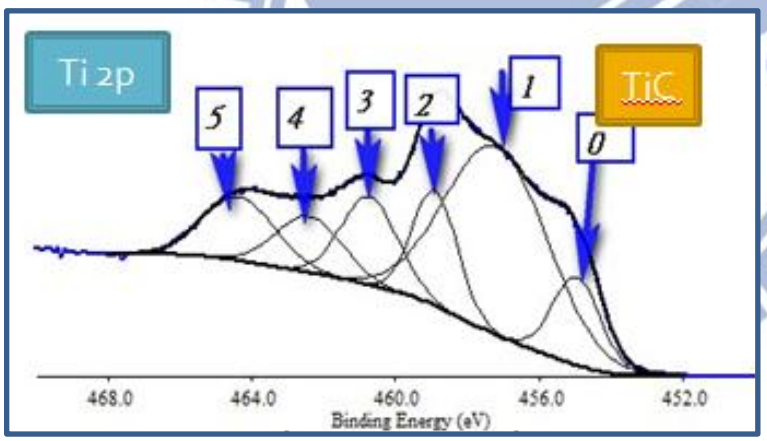

Fig. 4.6 XPS of Ti 2p (TiO_2 with 2% carbon).

Peak	Position (eV)	element or bonding
0	454.956	**TiC** $2p_{3/2}$
1	457.176	Ti_2O_3 $2p_{3/2}$
2	458.904	TiO_2 $2p_{3/2}$
3	460.728	TiO $2p_{1/2}$
4	462.416	Ti_2O_3 $2p_{1/2}$
5	464.376	TiO_2 $2p_{1/2}$

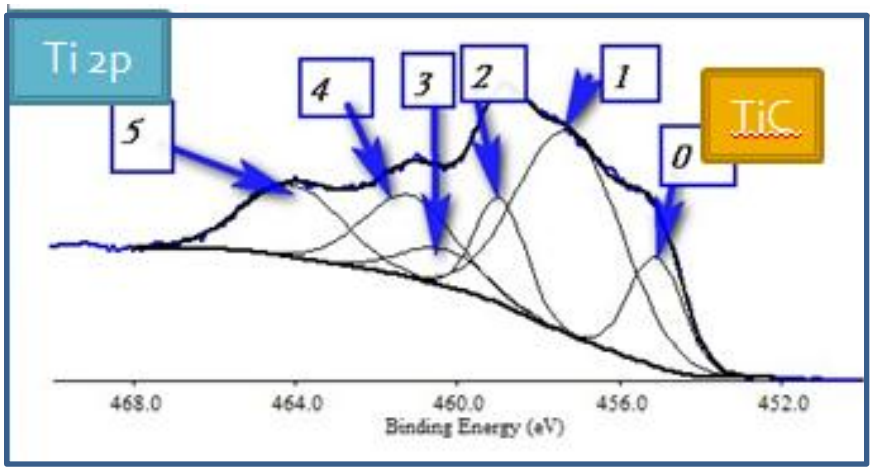

Fig. 4.7 XPS of Ti 2p (TiO_2 with 5% carbon).

Peak	Position (eV)	element or bonding
0	455.087	**TiC** $2p_{3/2}$
1	457.233	Ti_2O_3 $2p_{3/2}$
2	458.941	TiO_2 $2p_{3/2}$
3	460.342	TiO $2p_{1/2}$
4	461.175	TiO $2p_{1/2}$
5	464.069	TiO_2 $2p_{1/2}$

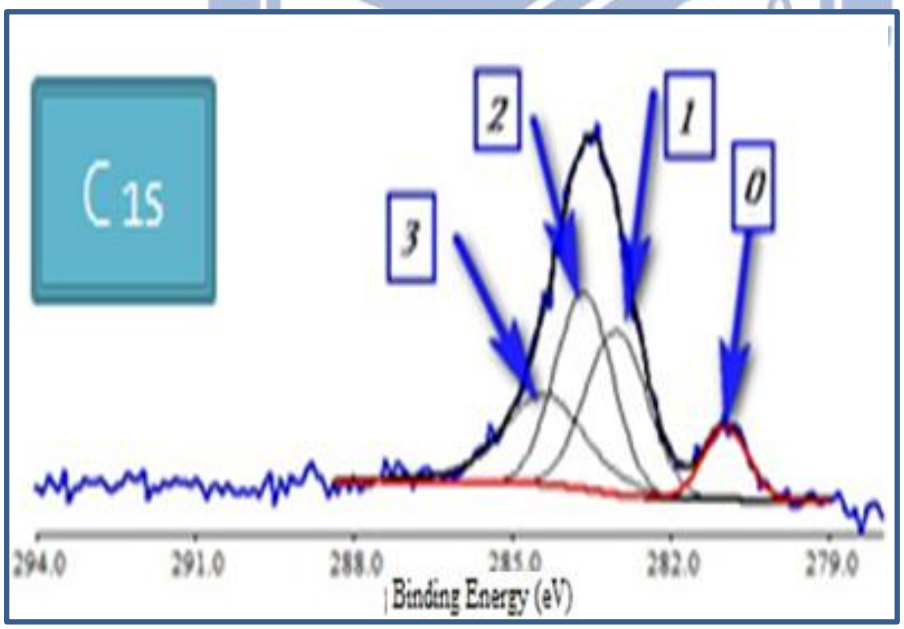

Fig. 4.8 XPS of C 1s (TiO_2 with 0% carbon).

Peak	Position (eV)	element or bonding
0	280.961	Sr $3p_{1/2}$
1	283.028	CO/Ti
2	283.648	CO
3	284.396	Carbon

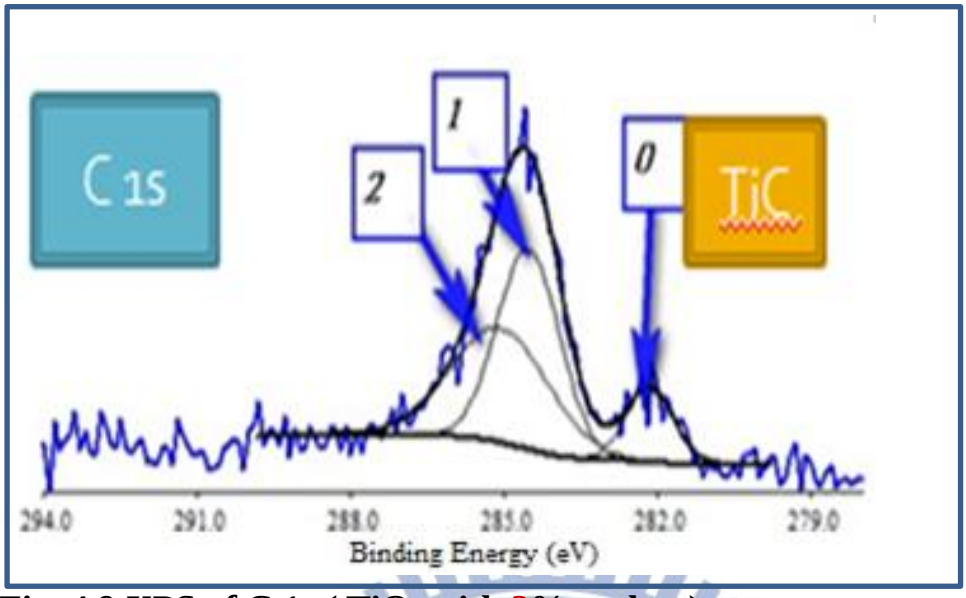

Fig. 4.9 XPS of C 1s (TiO_2 with 2% carbon).

Peak	Position (eV)	element or bonding
0	282.148	**TiC**
1	284.520	Hydrocarbon contaminated
2	285.079	Carbon contaminated from atmosphere

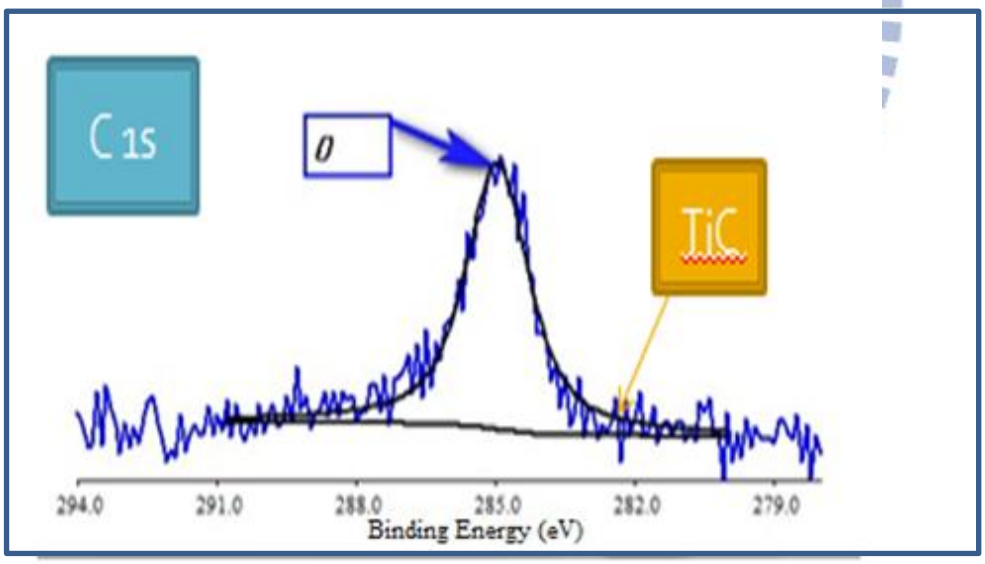

Fig. 4.10 XPS of C 1s (TiO_2 with 5% carbon).

Peak	Position (eV)	element or bonding
0	284.963	Carbon

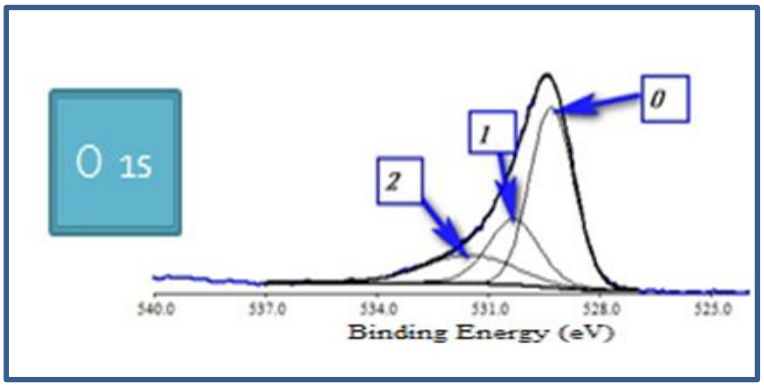

Fig. 4.11 XPS of O 1s (TiO_2 with 0% carbon).

Peak	Position (eV)	element or bonding
0	529.299	$SrTiO_3$
1	530.321	TiO_2
2	531.505	O_2

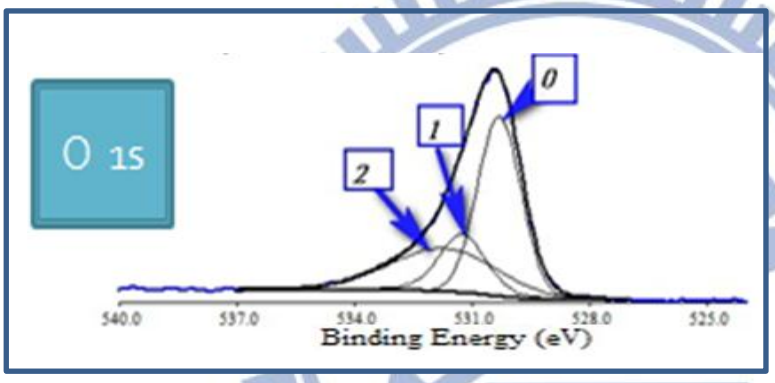

Fig. 4.12 XPS of O 1s (TiO_2 with 2% carbon).

Peak	Position (eV)	element or bonding
0	530.306	TiO_2
1	531.252	O_2
2	531.739	O_2

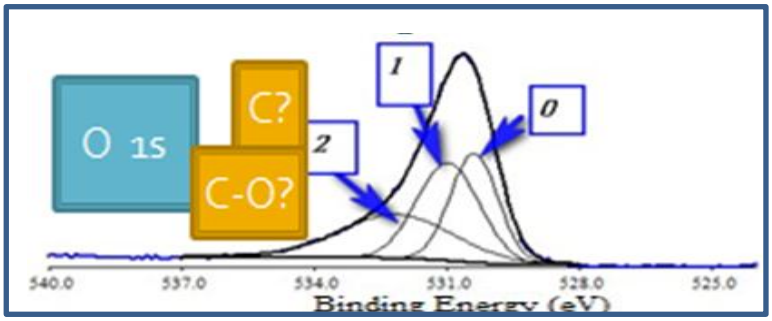

Fig. 4.13 XPS of O 1s (TiO_2 with 5% carbon).

Peak	Position (eV)	element or bonding
0	530.381	TiO_2
1	530.972	TiO_2
2	532.145	**Rh6(CO)16/C**

4-4 Diamagnetic effect caused by excessive carbon

We turn our attention to the magnetic moments of carbon, and compare the magnetic moment of TiO_2 with 2%, and 5% carbon. We use the magnetic moment of TiO_2 thin film with 2% carbon minus the the magnetic moment of TiO_2 thin film with 5% carbon and get a difference between them, then we compare the difference with the magnetic moment caused with pure 3% carbon concentration.

From Fig. 4.14, we can clearly know the effect of 3% carbon concentration, the diamagnetism caused by 3% carbon concentration **(Black line)** is significantly greater than the difference of the magnetic moment of TiO_2 thin film with 5% carbon subtracts the magnetic moment of TiO_2 thin film with 2% carbon **(Green line)**.

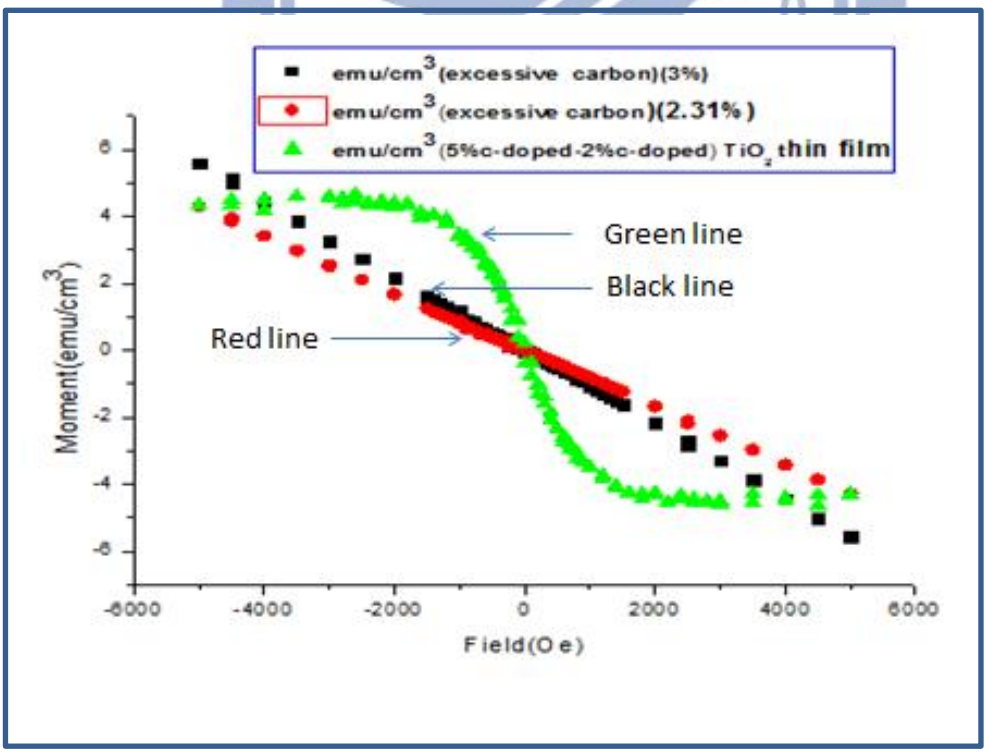

Fig. 4.14 Analysis of excessive magnetic moment.

Then, we investigate the two curves **(Black line and Green line)**. Because of hysteresis, the M-H curve of carbon-doped TiO_2 show ferromagnetism when we apply a small amount of magnetic field. To our knowledge, the characteristic of ferromagnetism is apparently different from diamagnetism. Therefore, it is not appropriate to compare the difference between the pure carbon and carbon-doped TiO_2 of the small amount of magnetic field. On the contrary, we put our attention to the ending point (+5000Oe and -5000Oe) of M-H curve, we want to know whether the excessive 3% carbon completely contribute the diamagnetism from the ending point of M–H curve. According to our calculations, we make the black line multiply a factor for the purpose of getting the same amount with saturation magnetization (Ms) with the magnetic moment between TiO_2 with 2% carbon and TiO_2 with 5% carbon **(Green line)**. We get the factor of 0.77, that is to say 2.31% (2.31=3×0.77) **(Red line)** is interstitial in the system and causes the excessive diamagnetism, namely it will reach saturation when we add 2.69% (5%-2.31%) carbon concentration in the carbon doped TiO_2 system.

However, about the **Rh6 (CO)16/C (Fig. 4.13) ,** if we regard it as pure carbon, it is not consistent with the normal peak of pure carbon, therefore we have to regard it as the bonding between carbon and oxygen, and we do a summary to explain the decrease of magnetic moment caused by the bonding between carbon and oxygen although we don’t have the correct information of magnetic moments of bonding between carbon and oxygen.

4-5 XANES analysis

For the purpose of increasing the convincing in the effect of carbon doping, we utilize the XANES to investigate our samples **(Fig. 4.15)**.

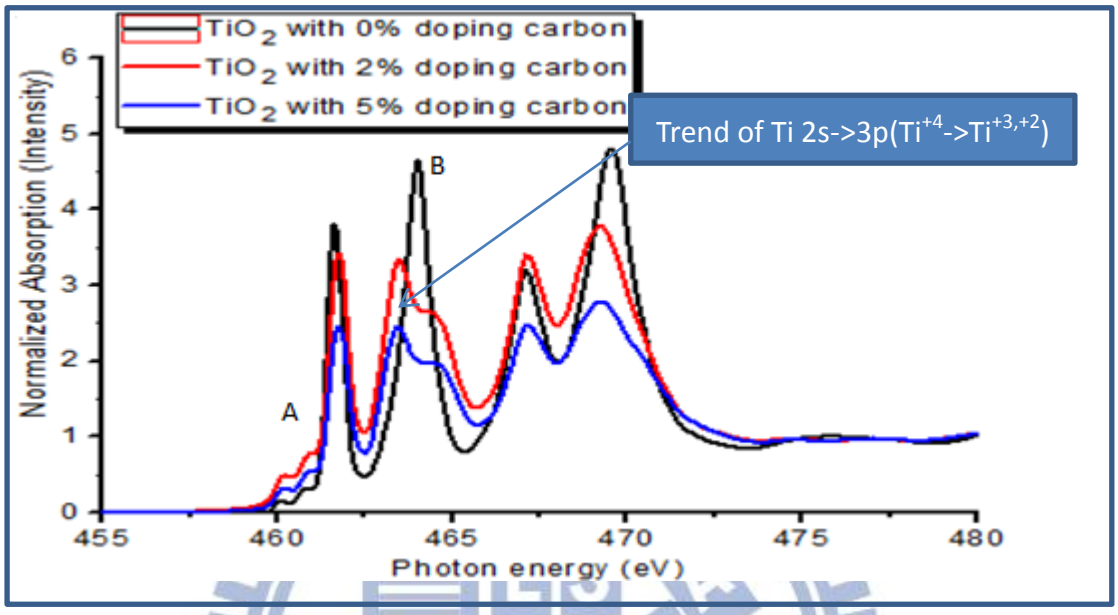

Fig. 4.15 The Ti L-edge XANES

We can obviously observe the contribution of carbon doping from **Fig. 4.15 "B" peaks,** the normalized absorption has the trend of decreasing with the increasing carbon doping concentration, the charge transition of Ti is from 3p to 4s and 3d in samples, it also means that Ti^{+4} will become Ti^{+3}or Ti^{+2}. Therefore it is a guarantee that the carbon actually entered into the system of carbon doped TiO_2.

On the other hand, we also can observe another result from "A" peaks**.** **I**n the progress from 0% to 2% doping, the A peak shifts to the right, it represents the lattice spacing between Ti and O expands, and it also means the rutile phase transfers into anatase phase.

We review the structure from Fig 1.11.

Rutile is tetragonal (a = 4.59 Å and c = 2.96 Å), while the anatase phase also crystallizes in a tetragonal structure (a = 3.78 Å and c = 9.52 Å).

However, in the progress from 2% to 5% doping, the peak shifts to the left, it represents the lattice spacing between Ti and O reduces, the opposite trend is abnormal that we can explain the abnormal magnetic moment is due to the variance of lattice spacing.

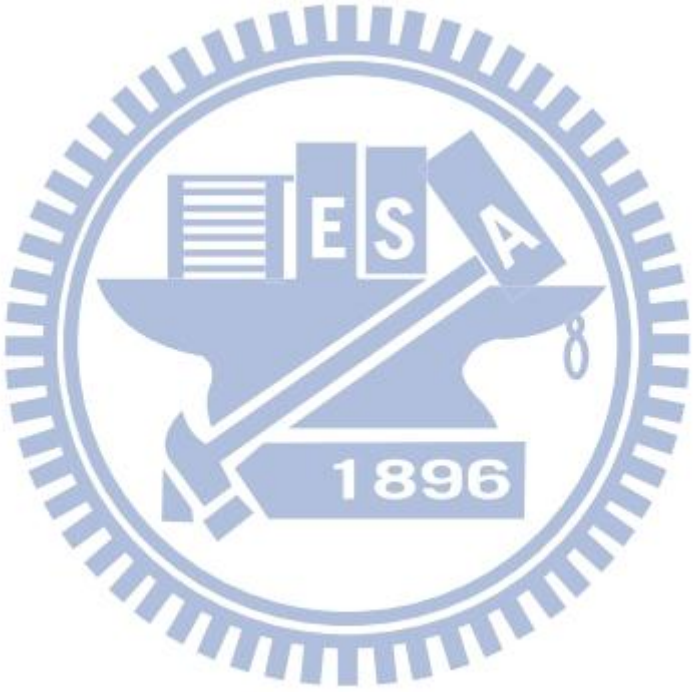

Chapter 5

Conclusions

1. We extend the research of carbon-doped TiO_2, and we prove that it is possible to form ferromagnetism even with thin films in anatase phase by choosing the appropriate procedures and conditions.

2. We get anatase (004) phase in thin film according to the observation from XRD. That is to say we can transfer powders of rutile phase into thin films of anatase phase by doping more carbon, or we can conclude that doping carbon is helpful to make anatase phase more stable. Namely it has potential to integrate the fields of magnetism and photocatalyst.

3. We can see the effect of oxygen vacancies by XPS. What's more, we also observe the phenomenon of Ti-C bonding. That is to say the Ti-C bonding also plays a significant role in inducing ferromagnetism.

4. In the doping process of 2% carbon doping to 5% carbon doping, the ferromagnetism shows the trend of decreasing, and we discovered the component **Rh6 (CO)16/C** by XPS**. I**f we regard it as pure carbon, that is to say the decrease of magnetic moment is caused by pure carbon, and we assume that it reach saturation in the process, the excessive carbon is interstitial in this system and causes the diamagnetism which decreases ferromagnetism. Through XPS, we can clearly observe that the system

exist the excessive component or bonding of carbon, it is consistent with our results and proves that saturation will be reached by carbon concentration about 2.69% (5%-2.31%) if the excess magnetic moment is all caused by carbon.

5. If we regard **Rh6 (CO)16/C** as pure carbon, it is not consistent with the normal peak of pure carbon, therefore we have to regard it as the bonding between carbon and oxygen, and summarize that the decrease in magnetic moment is caused by the **bonding** between carbon and oxygen. As for what exactly the bonding is due to, it might be a good topic of research for the future.

6. According to the XANES analysis, we confirm that the carbon actually entered into the system of carbon.
The Ti L-edge XANES **(Fig. 4.15)** means that Ti^{+4} will become Ti^{+3}or Ti^{+2} which is consistent with the productions of oxygen vacancies.
Then we elaborate the abnormal variance of magnetic moment is due to the variance of peak “A”.

Our work demonstrates that the magnetic moment is not absolutely positively correlated with the carbon doping concentration. If we dope too much carbon, it is possible to cause defects in our materials.

References

[1] 黃榮俊, 自旋電子之研究與發展, 物理雙月刊（廿六卷四期）.

[2] 胡裕民, III-V稀磁性半導體薄膜之研究與發展, 物理雙月刊（廿六卷四期）.

[3] H. Ohno, *Science* 281, 951 (1998).

[4] J. K. Furdyna and J. Kossut, *Diluted Magnetic Semiconductors*, vol. 25 of *Semiconductor and Semimetals* (Academic Press, New York, 1988); T. Dietl, (North-Holland, New York, 1994).

[5] A. Haury , A. Wasiela , A. Arnoult , J. Cibert , S. Tatarenko , T. Dietl , and Y. Merle d'Aubigné , *Phys. Rev. Lett.*79, 511 (1997).

[6] Toshio Kamiya and Masashi Kawasaki: MRS Bulletin, 33, 1061-1066, (2008).

[7] N. S. Gillis*,T. R. Koehler, Phys. Rev. Lett. 29, 369–372 (1972).

[8] H. Munekata, H. Ohno, S. von Molnar, Armin Segmüller, L. L. Chang, and L. Esaki, Phys. Rev. Lett. 63, 1849(1989).

[9] T. Dietl, H. Ohno, F. Matsukura, J. Cibert, D. Ferrand, *Science* 287, 1019 (2000).

[10] Sato K and Katayama-Yoshida H, *Japan. J. Appl. Phys.* 39 L555 (2000).

[11] Matsumoto Y, Murakami M, Shono T, Hasegawa T, Fukumara T, Kawasaki M, Ahmet P, Chikyow T, Koshihara S Y and Koinuma H, *Science* 291 854 (2001).

[12] M. L. Reed, N. A. El-Masry, H. H. Stadelmaier, M. K. Ritums, M. J. Reed, C. A. Parker, J. C. Roberts, and S. M. Bedair, Appl. Phys. Lett. 79, 3473 (2001).

[13] M.L. Reed a, M.K. Ritums a, H.H. Stadelmaier a,), M.J. Reed a, C.A. Parker b, S.M. Bedair b, N.A. El-Masry a , Mater. Lett. 51, 500 (2001).

[14] Saki Sonodaa*, Saburo Shimizua, Takahiko Sasakib, Yoshiyuki Yamamotob, Hidenobu Horia, J. Crystal Growth 237-239, 1358 (2002).

[15] M. Hashimoto, Y.K. Zhou, H. Tampo, M. Kanamura, H. Asahi*, J. Crystal Growth 252, 499 (2003).

[16] Kenji Ueda, Hitoshi Tabata, and Tomoji Kawa, Appl. Phys. Lett. 79, 988 (2001).

[17] Parmanand Sharma et al. , J. Magn. Magn. Mater. In Press, Uncorrected Proof, Available online 5 May 2004.

[18] R. A. de Groot , F. M. Mueller , P. G. van Engen and K. H. J. Buschow , *Phys. Rev. Lett.* 50, 2024 (1983).

[19] S. M. Watts, S. Wirth, S. von Molnár , A. Barry and J. M. D. Coey , *Phys. Rev B* 61, 9621 (2000).

[20] J.-H. Park, E. Vescovo, H.-J. Kim, C. Kwon, R. Ramesh & T. Venkatesan , *Nature* 392, 794, (1998).

[21] J. J. Versluijs, M. A. Bari, J. M. D. Coey, *Phys. Rev. Lett*. 87, 026601 (2001).

[22] K.-I. Kobayashi*, T. Kimura*, H. Sawada*, K. Terakura* & Y. Tokura* , *Nature* 395, 677 (1999).

[23] R P Borges, R M Thomas, C Cullinan, J M D Coey, R Suryanarayanan, L Ben-Dor, L Pinsard-Gaudart and A Revcolevschi, J. Phys.: C M 11, 445-L450 (1999).
[24] Y.Matsumoto, M. Murakami,T. Shono, T.Hasegawa,T. Fukumura,M. Kawasaki, P. Ahmet, T.Chikyow, S.-Y. Koshihara, and H. Koinuma, Science, 291, 854 (2001)
[25] S. A. Chambers, S. Thevuthasan, R. F. C. Farrow, R. F. Marks, J. U. Thiele, L. Folks, M. G. Samant, A. J. Kellock, N. Ruzycki, D. L. Ederer, and U. Diebold, Appl. Phys. Lett. 79, 3467 (2001).
[26] W. K. Park, R. J. Ortega-Hertogs, J. Moodera, A. Punnoose, and M. S. Seehra, J. Appl. Phys. 91, 8093 (2002).
[27] Yuji Matsumoto, Ryota Takahashi, Makoto Murakami, Takashi Koida, Xiao-Juan Fan, Tetsuya Hasegawa, Tomoteru Fukumura, M. Kawasaki, Shin-Ya Koshihara and Hideomi Koinuma', Jpn. J. Appl. Phys., Part 2 40, L1204 (2001).
[28] Y. Matsumoto, M. Murakami, T. Hasegawa, T. Fukumura, M. Kawasaki, P. Ahmet, K. Nakajima, T. Chikyow, and H. Koinuma, Appl. Surf. Sci. **189**, 344 (2002).
[29] S. A. Chambers, T. Droubay, C. M. Wang, A. S. Leab, R. F. C. Farrow, L. Folks, V. Deline, and S. Anders, Appl. Phys. Lett. **82**, 1257 (2003).
[30] A. Punnoose, M. S. Seehra, W. K. Park and J. S. Mooera, J. Appl. Phys. 93,7867 (2003).
[31] R. J. Kennedy and P. A. Stampe Erhong Hu, Peng Xiong, and Stephan von Molna and Yan Xin, Appl. Phys. Lett. 84, 2832 (2004).
[32] Nguyen Hoa Hong, Joe Sakai, and Awatef Hassini, Appl. Phys. Lett. 84, 2602 (2004).
[33] K. A. Griffin, A. B. Pakhomov, C. M. Wang, S. M. Heald, and Kannan M. Krishnan, Phys. Rev. Lett. 94,157204 (2005).
[34] Nguyen Hoa Hong, W. Prellier, Joe Sakai, and Awatef Hassin, Appl. Phys. Lett. 84, 2850 (2004).
[35] Mariana Weissmann, Leonardo A. Erric, P R B. 398, 179 (2007).
[36] S. J. Wang, W.-T. Chang, J.-Y. Ciou, M.-K. Wei*, and M. S. Wong, "Preparation of TiO2 thin films by laser ablation for photocatalytic applications", J. Vac. Sci. Technol. A, Vol. 26, 898-902 (2008).
[37] Tang H, Berger H, Schmid P E and Levy F 1994 *Solid State Commun.* 92 267 (1994).
[38] Hsieh C C, Wu K H, Juang J Y, Uen T M, Lin J-Y and Gou Y S 2002 *J. Appl. Phys.* 92 2518 (2002).
[39] Murakami M, Matsumoto Y, Nakajima K, Makino T, Segawa Y, Chikyow T, Ahmet P, Kawasaki M and Koinuma H 2001 *Appl. Phys. Lett.* 78 2664 (2001).
[40] Kennedy R J and Stampe P A 2003 *J. Cryst. Growth* 252 333 (2003).

[41] Parker N J, Kharel P, Powell J R, Smith P A, Evans P D and Porch A 1999 *IEEE Trans. Appl. Supercond.* 9 1928 (1999).
[42] Zuccaro C, Ghosh I, Urban K, Klein N, Penn S and Alford N M 1997 *IEEE Trans. Appl. Supercond.* 7 3715 (1997).
[43] Augustynski J 1993 *J. Electronchim. Acta* 38 43 (1993).
[44] *W.Prellier, A.Fouchet and B.Mercey, J.Phys.: Condens. Matter. 15 R1583-R1601* (*2003).*
[45] C.-F. Yu, T.-J. Lin, S.-J. Sun, and H. Chou, *J. Phys. D* 40, 6497 (2007).
[46] H. Pan, J. B. Yi, L. Shen, R. Q. Wu, J. H. Yang, J. Y. Lin, Y. P. Feng, J. Ding, L. H. Van, and J. H. Yin, *Phys. Rev. Lett.* 99, 127201 (2007).
[47] S. Zhou, Q. Xu, K. Potzger, G. Talut, R. Groetzschel, J. Fassbender, M. Vinnichenko, J. Grenzer, M. Helm, H. Hochmuth, M. Lorenz, M. Grundmann, and H. Schmidt, *Appl. Phys. Lett.* 93. 232507 (2008).
[48] J. J. Attema, G. A. de Wijs, G. R. Blake, and R. A. de Groot, *J. Am. Chem. Soc.* 127, 16325 (2005).
[49] L. Shen, R. Q. Wu, H. Pan, G. W. Peng, M. Yang, Z. D. Sha, and Y. P. Feng, *Phys. Rev. B* 78, 073306 (2008).
[50] Kesong Yang, Ying Dai, Baibiao Huang, and M. H. Whangbo, *Appl. Phys. Lett.* 93, 132507 (2008).
[51] Abdul K. Rumaiz, J. C. Woicik, E. Cockayne, H. Y. Lin, G. Hassnain Jaffari, and S. I. Shah, *Appl. Phys. Lett.* 93, 262111 (2009).
[52] J. M. D. Coey, Kwanruthai Wongsaprom, J. Alaria, and M. Venkatesan, *J. Phys. D: Appl. Phys.* 41, 134012 (2008).
[53] 宛德福、馬興隆，磁性物理學，電子工業出版社 (1999).
[54] 戴道生、錢昆明等等，鐵磁學，科學出版社 (2000).